OPERATIONAL CLOUD-TO-GROUND LIGHTNING INITIATION FORECASTING UTILIZING S-BAND DUAL-POLARIZATION RADAR

THESIS

Kyle R. Thurmond, Captain, USAF

AFIT-ENP-14-M-36

DEPARTMENT OF THE AIR FORCE
AIR UNIVERSITY

AIR FORCE INSTITUTE OF TECHNOLOGY

Wright-Patterson Air Force Base, Ohio

AFIT-ENP-14-M-36

OPERATIONAL CLOUD-TO-GROUND LIGHTNING INITIATION FORECASTING UTILIZING S-BAND DUAL-POLARIZATION RADAR

THESIS

Presented to the Faculty

Department of Engineering and Physics

Graduate School of Engineering and Management

Air Force Institute of Technology

Air University

Air Education and Training Command

In Partial Fulfillment of the Requirements for the

Degree of Master of Science in Applied Physics

Kyle R. Thurmond, BS

Captain, USAF

March 2014

AFIT-ENP-14-M-36

OPERATIONAL CLOUD-TO-GROUND LIGHTNING INITIATION FORECASTING UTILIZING S-BAND DUAL-POLARIZATION RADAR

Kyle R. Thurmond, BS
Captain, USAF

Approved:

//signed//   17 Mar 14
_____   _____
Kevin S. Bartlett, Lt Col, USAF (Chairman)   Date

//signed//   17 Mar 14
_____   _____
Robert S. Wacker, Lt Col, USAF (Member)   Date

//signed//   17 Mar 14
_____   _____
Ariel O. Acebal, PhD (Member)   Date

AFIT-ENP-14-M-36

Abstract

Previous research on cloud-to-ground (CG) lightning initiation forecasting shows a potential benefit in using dual-polarization (DP) weather radar. The propagation of radio waves in both the horizontal and vertical planes makes DP radar better equipped to identify radar returns indicative of charge separation within clouds. Algorithms using the DP radar products of differential reflectivity (Z_{DR}) and specific differential phase (K_{DP}) combined with reflectivity (Z) values were developed to determine if DP radar could outperform a standard conventional radar forecasting technique ($Z \geq 40\text{dBZ}$ at $-10°\text{C}$). 68 single-cell thunderstorms were evaluated near Kennedy Space Center (KSC), FL for to develop and test these algorithms. It was concluded that using DP radar to forecast CG lightning provided better results than the standard conventional radar technique through improved skill scores (100% possibility of detection and 0% false alarm ratio), increased lead time (approximately 5 minutes), or both. However, more research over a longer time period is needed to validate these results and convert to an automated operational forecasting tool.

Acknowledgments

I would first like to thank my committee chair Lt Col. Kevin Bartlett and my committee members Lt Col. Robert Wacker and Dr. Ariel Acebal for their time, patience, and continual assistance in guiding me through the process of researching and writing this thesis. Additionally I would like to extend my gratitude to Mr. William Roeder at the 45th Weather Squadron (45 WS) for his help in this topic and the work he did to set up a two day site visit to observe the forecasting process at the 45 WS and tour the facilities. I would also like to thank my mom and dad for their lifelong sacrifices that have directed on the path to enhance my education and personal development. Lastly I would like to thank my wonderful wife for her words of affection, praise, and encouragement, her deep friendship, and incredible love over these past two years at the Air Force Institute of Technology.

Kyle R. Thurmond

Table of Contents

List of Figures

List of Tables

OPERATIONAL CLOUD-TO-GROUND LIGHTNING INITIATION FORECASTING

UTILIZING S-BAND DUAL-POLARIZATION RADAR

I. Introduction

The 45th Weather Squadron (45 WS) provides comprehensive weather service to Cape Canaveral Air Force Station (CCAFS), Patrick Air Force Base, and Kennedy Space Center (KSC), FL in support of the United States' space program. These services include but are not limited to providing weather forecasts for over 30 space launches per year by the Department of Defense (DoD), National Aeronautics and Space Administration (NASA), and commercial launch customers (Roeder et al., 2005). Therefore, the 45 WS has a difficult task of providing weather support to CCAFS/KSC due to launch operation weather sensitivities and frequent lightning activity in the area. The state of Florida records the most lightning flashes per year of any state, and central Florida is the location of the country's area of highest lightning activity known as "lightning alley" (Roeder et al., 2005; Weems et al., 2001). Advance ground processing for space launch at KSC can begin with rockets and payloads at the launch pads weeks or even months before launch. This puts KSC space launch operations at high risk to lightning producing storms that can form in as little as 20-30 minutes in the summer months over central Florida (Roeder et al., 2005)

A lightning strike to a launch vehicle or pad holding fuel and equipment could cause billions of dollars of damage, serious injury, or loss of life. Additionally, lightning strikes that hit the ground near the launch pad can induce electrical currents that can damage equipment on the launch pad when not safeguarded properly (Roeder and Saul,

2012; Roeder et al., 2005). The 45 WS issues over 1,500 lightning advisories per year, which are a large contributor to space launch delays and cancellations. From 1 January 1988 to 1 June 2005, one-third of launches were delayed and one-third were scrubbed while approximately one-third of those delayed and half of the scrubbed missions were due to weather (Roeder et al., 2005). Since lightning impacts such a high percentage of their launches, the 45 WS desires a new method to forecast lightning initiation with better accuracy and increased lead time.

The forecasting method chosen for this study was to use the National Weather Service's (NWS) Melbourne, Florida S-band Weather Surveillance Radar-1988 Doppler (WSR-88D) (KMLB), upgraded to dual-polarization (DP) capability in January 2012, to analyze single-cell thunderstorms near CCAFS/KSC. The United States' WSR-88D radar network upgrade to DP capabilities was completed in 2013; therefore the use of DP radar is still a relatively new tool to most weather forecasters (Kumjian, 2013a). To date, no lightning initiation studies using DP radar have been conducted near CCAFS/KSC. This study compares a preexisting cloud-to-ground (CG) lightning initiation forecasting technique, using conventional radar with horizontal reflectivity, to forecasting techniques created through added resources of the DP radar variables, specifically differential reflectivity (Z_{DR}) and specific differential phase (K_{DP}).

Since the use of DP radar is new, all its added benefits and limitations have not been discovered. Some benefits of DP radar over conventional radar include but are not limited to improved capability to determine precipitation types (hydrometeors), distinguish between meteorological and non-meteorological targets like insects, as well as better precipitation estimates, and improved melting layer, hail and tornadic debris

identification within severe thunderstorms (Kumjian, 2013a; 2013b; 2013c). This research was accomplished to determine the operational utility of DP radar to improve CG lightning initiation forecasting at CCAFS/KSC. It was hypothesized that the added capabilities of Z_{DR} and K_{DP} would improve the user's ability to identify hydrometeor signatures known for thunderstorm charging. DP capabilities should enable the development of CG lightning initiation forecasting techniques that outperform existing forecasting techniques used by conventional radar. The chapters that follow will introduce thunderstorm and lightning formation processes as well as discuss previous research that has been conducted in the study of CG lightning initiation. The research methodology will be described while the added benefits of DP radar forecasting techniques will be explained in both the results and conclusion chapters.

II. Background

2.1 Convective Development of a Single-Cell Thunderstorm

Thunderstorms can form due to multiple processes including low level convergence, thermal convection, and forced lifting by fronts or local topography. This study focuses specifically on pulse thunderstorms, or single-cell thunderstorms, created through convection.   These thunderstorms are frequent in Florida and enable unambiguous correlation of radar reflectivity and detected lightning. A single-cell thunderstorm is defined as an isolated cumulonimbus cloud that forms within an unstable airmass under conditions of weak vertical wind shear by localized thermal convection (Wallace and Hobbs, 2006). These storms often are triggered by weak upward motions forced by moving low-level boundaries and/or flow moving over these boundaries. Examples of these low-level boundaries during summer in central Florida include sea breeze fronts off the Atlantic Ocean and Gulf of Mexico, river breeze fronts off the Indian River and Banana River in the CCAFS/KSC area, convective outflows, frictional convergences, horizontal convective rolls, and lake breezes. Even thermal circulations from discontinuities in soil moisture or cloud shadows have been observed to play a role. Thunderstorms are more likely to form where two or more of these boundaries intersect (Roeder et al., 2011; 2005; 1998). The first detailed study of convective single-cell thunderstorms, the Thunderstorm Project, was conducted in 1948. During this project P-61 instrumented aircraft penetrated thunderstorms in Ohio and Florida. This study produced the generally-accepted three-stage life cycle of single-cell thunderstorm development: the cumulus, mature, and dissipating stages (Wallace and Hobbs, 2006;

Doswell, 2001; MacGorman and Rust, 1998; Rogers and Yau, 1989; Byers and Braham, 1949) as seen in Figure 1.
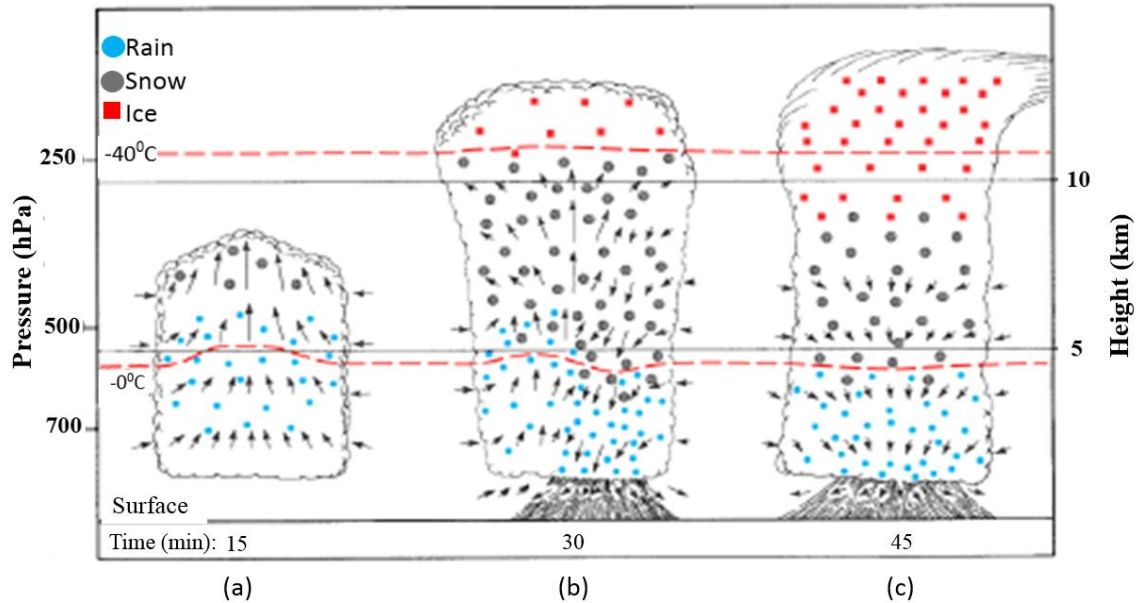
Figure 1: Schematic of the typical three-stage life cycle of a single-cell thunderstorm: (a) cumulus stage, (b) mature stage, (c) dissipating stage. From Wallace and Hobbs, 2006. Used by permission.

The cumulous stage consists of warm buoyant air rising allowing water to condense on cloud condensation nuclei. Cloud droplets grow by collisions and coalescence of the droplets (Wallace and Hobbs, 2006; Rogers and Yau, 1989). This stage is characterized by increasing vertical velocities within the updraft. Vertical velocities near the cloud top can reach approximately 10ms^{-1} (Wallace and Hobbs, 2006; Doswell, 2001). As the cloud top increases in height, the strength of the updraft lofts supercooled raindrops above the freezing level, a key process in lightning initiation. At this point the cloud is approaching the mature stage and has been in the cumulus stage for approximately 15 minutes (Wallace and Hobbs, 2006; Rogers and Yau, 1989).

Once cloud droplet grow large enough they will begin to fall as precipitation and the storm enters the mature stage. The falling droplets create a downward drag force on the air around them, leading to the development of a downdraft. Dry environmental air is entrained into the top and sides of the downdraft causing falling precipitation to evaporate and cool the unsaturated air below the base of the cloud. The cell is then fully mature and is characterized by turbulent internal mixing with the strong updraft and downdraft in close proximity (Wallace and Hobbs, 2006; Rogers and Yau, 1989). Ice crystals begin to form at the top of the cloud as the storm continues to grow vertically into the upper troposphere. Supercooled droplets are still present above the freezing level while snowflakes and graupel (rimed particles consisting of a mixture of ice and water) can remain frozen for some distance below the freezing level in the downdraft (Wallace and Hobbs, 2006). This study focuses on the mature stage of a storm's life cycle. Cloud charging and lightning initiation occur during this stage in the mixed region where supercooled drops, ice, and graupel are present (Wallace and Hobbs, 2006; MacGorman and Rust, 1998). A typical storm takes about 30 minutes to pass the mature stage. The lack of vertical wind shear in the single-cell thunderstorm life cycle causes the downdraft to interfere with the updraft, transitioning the storm to the dissipating stage (Wallace and Hobbs, 2006; Rogers and Yau, 1989). During the dissipating stage the overshooting cloud top forms an anvil cloud along the tropopause. It takes approximately 30 minutes for the storm to completely decay into cloud debris (Wallace and Hobbs, 2006; Rogers and Yau, 1989).

2.2 Lightning Initiation in Single-Cell Thunderstorms

The mature stage of a single-cell thunderstorm is defined by the presence of both an updraft and a downdraft. Deierling et al. (2008, 2005) showed that lightning production is proportional to the upward mass flux of ice crystals and the downward mass flux of graupel. This leads to the formation of a vertical tripole charge structure. This simplified structure consists of a main negative charge zone between -10°C and -20°C positioned between positive charge regions near the cloud base and top (Wallace and Hobbs, 2006; MacGorman and Rust, 1998; Bringi et al., 1997; Ziegler and MacGorman, 1994; Marshall and Rust, 1991; Williams, 1989; Uman, 1987). While individual storm cells exhibit considerably more complexity in their charge distributions, the tripole model is adequate to explain lightning formation. Although charge regions exist from the cloud base to the cloud top, the main charging zone produces the most lightning, and is almost always the source of CG lightning initiation (Wallace and Hobbs, 2006; Carey and Rutledge, 2000; MacGorman and Rust, 1998; Williams, 1989; Uman, 1987; Dye et al., 1986, 1988; Krehbiel et al., 1979; Workman and Reynolds, 1949).

The triple structure is produced by collisions between graupel and ice crystals in the mixed-phase region of the cloud, where supercooled liquid water, graupel, and ice crystals coexist. This region occurs between approximately -10°C and -40°C (Yang and King, 2010; MacGorman and Rust, 1998). This graupel-ice interaction leads to noninductive charging (NIC), the most generally accepted explanation for thunderstorm charging (Yang and King, 2010; Carey and Rutledge, 2000, 1996; MacGorman and Rust, 1998; Rutledge and Petersen, 1994; Saunders et al., 1991; Keith and Saunders, 1990; Goodman et al., 1988; Dye et al., 1988, 1986; Takahashi, 1978; Church, 1966; Reynolds

et al., 1957). After collision, the colder and lighter ice crystal is typically positively

charged while the warmer and heavier graupel becomes negatively charged (Yang and

King, 2001; Reynolds et al., 1957). The ice crystals tend to be carried upward with the

updraft, taking positive charge with them to the top of the storm, while the heavier

negatively charged graupel fall through the updraft to the lower portion of the storm.

This acts to create a positive charged region at the storm top and negative charged region

towards the lower center of the storm defined earlier as the main charging zone (Yang

and King, 2010; MacGorman and Rust, 1998). Wallace and Hobbs (2006) speculate that

similar mixed-phase processes may create the secondary positive charge region near the

cloud base.

　　If enough charge is separated in the cloud, the electric field can intensify to the

point where dielectric breakdown occurs between charge regions or between a charge

region and the ground. This dielectric breakdown creates an ionized channel through

which charge flows until no electric potential difference remains. A lightning discharge

that occurs between clouds, within a cloud, or between the cloud and the surrounding air

is known as intracloud (IC) lightning (Wallace and Hobbs, 2006; MacGorman and Rust,

1998; Uman, 1987). The focus of this study, however, is cloud-to-ground (CG) lightning.

The initial discharge for CG lightning typically occurs between the main negative charge

region and the positive charge region induced below it on the ground (Uman, 1987).

2.3 Lightning Detection at CCAFS/KSC

　　Lightning watch and warning advisories (WWAs) are the most frequently issued

products by the 45 WS, averaging over 2,000 WWAs per year between 2002 and 2009

8

(Roeder et al., 2011). There are two reasons for the high number of advisories. The first is due to the frequency of thunderstorm activity in central Florida, and the second is that the 45 WS has overlapping areas of responsibility where advisories must be issued if lightning is predicted to occur. In total, there are 13 different locations, shown in Figure 2, that fall under the areas of responsibility for the 45 WS, each with a 5nmi radius (Roeder et al., 2011; Weems et al., 2001).
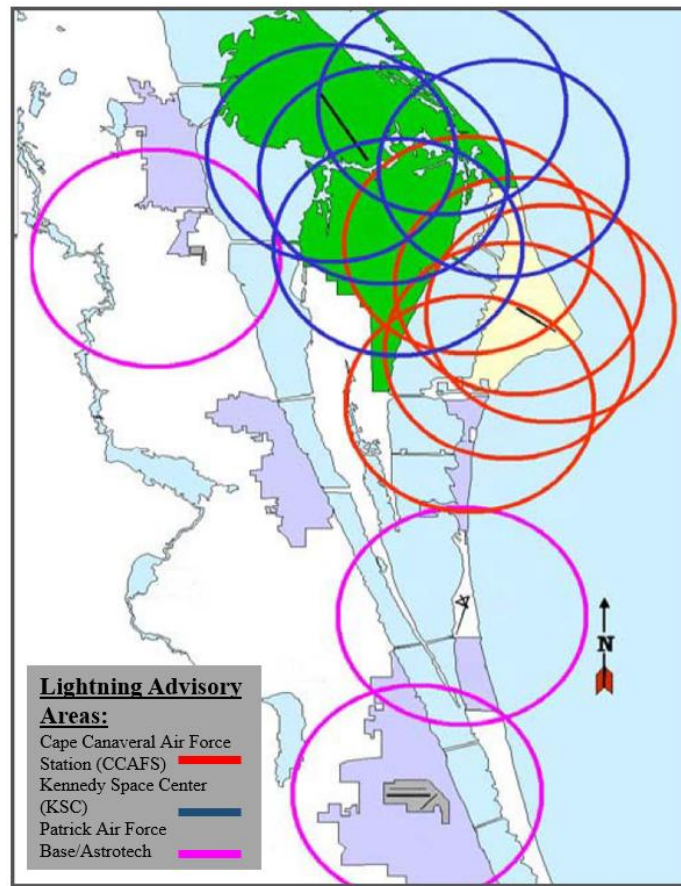
Figure 2: Map of the 13 locations the 45 Weather Squadron (45 WS) issues lightning watches and warnings for. Each area is a circle with a 5nmi radius. Red circles represent Cape Canaveral Air Force Station (CCAFS), blue circles represent Kennedy Space Center (KSC), and magenta circles represent Patrick Air Force Base (PAFB) and Astrotech. From Roeder et al., 2011. Used by permission.

There are two types of WWAs issued by the 45 WS. The first is a Phase-1 Lightning

Watch, which indicates that lightning is predicted within a 5nmi radius of the location

and has a desired lead time of 30 minutes. This watch is issued at the 45 WS based on IC

lightning potential to allow additional lead time for safety purposes, because CG

lightning does not typically occur until after IC is observed. The second, a Phase-2

Lightning Warning, indicates that CG lightning is imminent or occurring within 5nmi of

the location and does not have a desired lead time.

The 45 WS can detect lightning near these 13 locations through the use of their

Four Dimensional Lightning Surveillance System (4DLSS) (Roeder et al., 2011; Murphy

et al., 2008). The 4DLSS detects all types of lightning including IC lightning. The IC

component of 4DLSS consists of nine sensors on the ground dispersed between

CCAFS/KSC and is often referred to by its previous name, the Lightning Detection And

Ranging (LDAR), now LDAR-II (Weems et al., 2001). The CG lightning component of

4DLSS is often referred to by its previous name, the Cloud-to-Ground Lightning

Surveillance System (CGLSS), now CGLSS-2 (Roeder et al., 2011). A map of the six

CG lightning sensors used in the 4DLSS is shown in Figure 3.
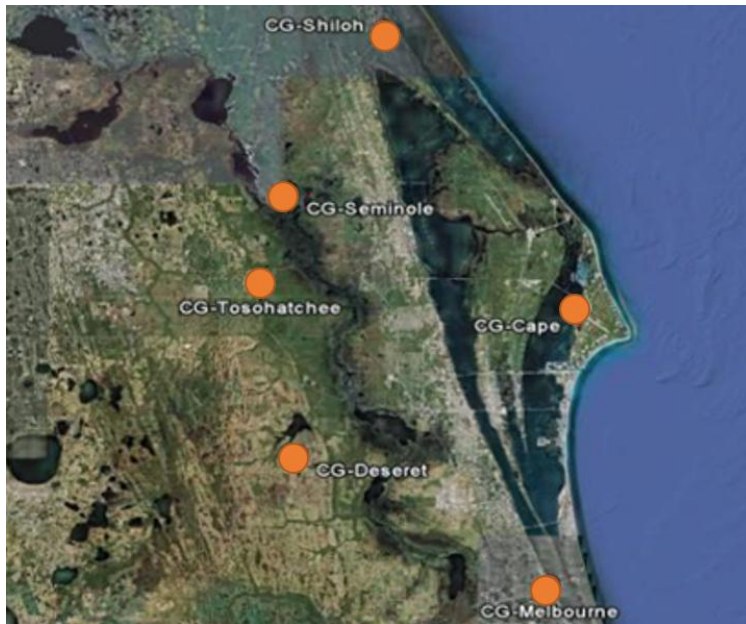
Figure 3: Map of the Four Dimensional Lightning Surveillance System (4DLSS) cloud-to-ground lightning sensor locations. From Roeder et al., 2011. Used by permission.

2.4 Radar Reflectivity Studies of Lightning Initiation

NIC leads to the formation of the tripole structure of a thunderstorm. This process, as mentioned earlier, relies on the interaction of hydrometeors such as ice crystals and graupel. Graupel, however, only begins to form when the updraft lofts supercooled drops above the freezing level. Therefore a general method for predicting lightning initiation was to identify storms that contain supercooled drop signatures above the freezing level for potential lightning initiation. However, before the introduction of dual-polarization (DP) radar, this could only be inferred by observing the precipitation core of a thunderstorm with high reflectivity (Z) values seen in single-polarization (SP) radar products.

A SP radar, here after referred to as a conventional radar, sends out pulses of electromagnetic (EM) radiation and receives return echoes from anything in the signal's path including but not limited to hydrometeors, smoke, and insects. The radar sends out a horizontally polarized wave that oscillates in the horizontal plane, parallel to the ground (Kumjian 2013a). When the EM wave interacts with a target in the atmosphere, the target scatters radiation in all directions with amplitude relative to its size, shape, and composition. Therefore the radar is capable of measuring how reflective a target or particle is to EM radiation (Kumjian 2013a; Rinehart, 2010). The most common conventional radar variable used in lightning prediction is reflectivity combined with an environmental temperature level, because increasing reflectivity values are proportional to increasing storm strength and the power received by the radar. The received power from a target is calculated using the Rayleigh scatter approximation since most hydrometeors are smaller than the radar wavelength. It is calculated by:

$$P_r = \frac{\pi^3 p_t g^2 \theta \phi h |K|^2 z}{1024 \ln(2) \lambda^2 r^2} \tag{1}$$

where λ represents the wavelength, p_t is the peak transmitter power, g is the antenna gain, θ and ϕ represent the horizontal and vertical beamwidths of the radar antenna, and h is the radar pulse length (Rinehart, 2010). Conventional radar specific constant variables are depicted in Table 1 for the Weather Surveillance Radar-1988 Doppler (WSR-88D).

Table 1: WSR-88D constants (Rinehart, 2010)

WSR-88D Constant Values	λ	p_t	g	θ and ϕ	h
Units	cm	kW	dB	degrees	μs
Value	10.71	1000	45	0.63	1.57, 4.5

$/K|^2$ is the dielectric constant term (typically 0.93 for water and 0.197 for ice), r is the

distance to the target, and the final term, z, is the radar reflectivity factor, which accounts

for the sum of all hydrometeors within the radar volume scan. Therefore, all the

constants of the WSR-88D can be combined into a single constant C_1 and the received

power from a target becomes:

$$p_r = \frac{C_1 z}{r^2} \tag{2}$$

Therefore the reflectivity factor can be written as $z = C_2 p_r r^2$, where C_2 is a radar constant

with value 64.90dB for the WSR-88D, and shows that the power received is proportional

to the radar reflectivity factor and inversely proportional to range squared (Rinehart,

2010). Thus, the stronger the storm, the higher the power received by the radar, and the

stronger the reflectivity factor. Lastly, for the same distance, reflectivity values range

multiple orders of magnitude which can be as low as $0.001 mm^6 m^{-3}$ for fog and as high a

$50,000,000 mm^6 m^{-3}$ for heavy hail. This wide range of values is difficult to work with, so

reflectivity is typically compressed into a more manageable range through the equation:

$$Z = 10 \log_{10} \left(\frac{z}{1\ mm^6/m^3} \right) \tag{3}$$

where Z is a logarithmic parameter known as reflectivity and is measured in dBZ while z is a linear parameter measured in mm^6m^{-3} (Rinehart, 2010).

Larger Z values indicate the presence of a strong updraft capable of lofting and maintaining supercooled drops above the freezing level (Rinehart, 2010). Correlation between Z values at or above specific thermal levels in the atmosphere has been used to predict CG lightning and has been the topic of multiple studies yielding many rules of thumb and forecasting techniques in use today. Previous research that has attempted to find the best possible Z value at or above a specified thermal level includes but is not limited to: Dye et al. (1989), Buechler and Goodman (1990), Zipser and Lutz (1994), Petersen et al. (1996), Roeder and Pinder (1998), Gremillion and Orville (1999), Vincent et al. (2003), Wolf (2006), Yang and King (2010), and Woodard (2011).

The most common result of these studies was that observing a reflectivity value of 40dBZ at or above approximately -10°C proved to be the most favorable forecasting technique for predicting CG lightning initiation. Dye et al. (1989) analyzed 20 storms in New Mexico and reported that the storms did not become electrically active (electrical fields inside the clouds exceeding $1kVm^{-1}$) until reflectivity values reached 40dBZ at approximately -10°C. Buechler and Goodman (1990) analyzed 15 storms in Alabama, Florida, and New Mexico and discovered if lightning was forecast upon observing 40dBZ at -10°C, then the forecast would give a 100% possibility of detection, a 7% false alarm rate, and a 93% critical skill index with lead times ranging from 3 to 33 minutes. Gremillion and Orville (1999) found that observing 40dBZ at -10°C produced the best statistical forecasting results and a median lead time of 7.5 minutes when analyzing 39 storms in Florida. Vincent et al. (2003) studied 50 storms in North Carolina and

discovered that observing 40dBZ at -10°C occurred on average 14.7 minutes before

lightning initiation while Wolf (2006) found the same threshold provided the best

statistical forecast results after analyzing 1,164 storms in Florida. Lastly, Yang and King

(2010) showed the best statistical forecast results and an average lead time of 17 minutes

came from observing 40dBZ at -10°C while studying 143 storms in southern Ontario. It

is worth noting that even though the majority of research studies found this threshold

favorable for lightning forecasting, it was not unanimous. For example Mosier et al.

(2011) determined that the best statistical forecasting results came from paring two

consecutive radar volumes scans of $Z \geq 30dBZ$ at -15°C when analyzing over 67,000

storms in the summer months of Texas from 1997 to 2006.

2.5 Dual-Polarization Radar Products

The radar used in this study was the National Weather Service's (NWS) WSR-

88D in Melbourne, Florida (KMLB) which is approximately 30 miles south of most of

the launch pads used at CCAFS/KSC. In January 2012 KMLB was upgraded to function

as a DP radar. The 45 WS has access to a closer Air Force operated radar (a modified

WSR-74C) located at Patrick Air Force Base approximately 20 miles south-southwest

from the majority of the launch pads used by CCAFS/KSC, however, this radar was

under maintenance during study (Roeder et al., 2011). Both radar locations are shown in

Figure 4.
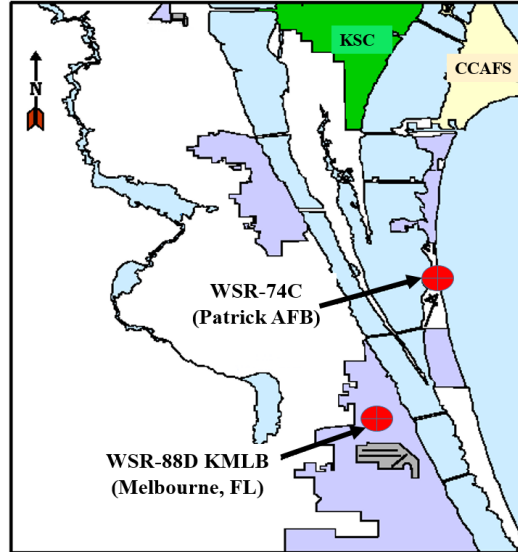
Figure 4: Radar location map. Map of KMLB in Melbourne, FL and the WSR-74C located at Patrick AFB relative to CCAFS/KSC. From Roeder et al., 2011. Used by Permission.

This study used KMLB to identify lightning initiation through measured precipitation returns; therefore a basic knowledge of DP radar precipitation measurement is needed. To do this, the characteristics of the WSR-88D along with differential reflectivity (Z_{DR}), differential phase (Φ_{DP}), and specific differential phase (K_{DP}) will be discussed.

When a particle is illuminated by a horizontally polarized EM wave, the particle acts as a horizontal dipole antenna and scatters energy with horizontal polarization. In the same way when a vertically polarized EM wave illuminates a particle, the particle acts as a vertical dipole antenna and scatters energy with vertical polarization. The DP WSR-88D transmits EM radiation with both vertical and horizontal polarization in a single pulse and compares the return signals at each polarization. Information about the size, shape, and orientation of hydrometeors within the radar's sampling volume can be interpreted through this received backscatter (Kumjian, 2013a). One of the two DP radar

products used in this study to forecast lightning was Differential reflectivity (Z_{DR}), which is calculated as the ratio of the backscattered horizontal and vertical reflectivity factors with the following equation:

$$Z_{DR} = 10\log_{10}\frac{z_h}{z_V} \tag{4}$$

where z_h is the reflectivity factor measured in the horizontal plane and z_v is the reflectivity factor measured in the vertical plane. The units for both the horizontal and vertical reflectivity factors are $mm^6 \, m^{-3}$ while Z_{DR} is measured in dB (Rinehart, 2010). Hydrometeors like large rain drops and water coated ice are typically larger in the horizontal than in the vertical due to aerodynamic forces, thus giving Z_{DR} a positive value. Small raindrops such as drizzle or tumbling hail are either spherical or appear to be spherical on average, respectively, and therefore return a Z_{DR} value near zero. Hydrometeors such as vertically oriented ice crystals produce negative values since their return in the vertical is larger than the horizontal (Kumjian, 2013a; Rinehart, 2010).

The second DP radar product used in this study is specific differential phase (K_{DP}), however, it can only be explained by first examining differential phase (Φ_{DP}). EM radiation does not travel through different precipitation types at constant speed. A horizontally polarized radar signal will be slowed more than a vertically polarized radar signal when propagating through an environment of oblate raindrops (Kumjian, 2013a). The horizontal signal lags behind the vertical signal and the change in phase can be measured by the DP radar. This lag, or Φ_{DP}, is defined as a difference in phase shift between horizontal and vertical polarizations. It is measured in degrees and is calculated with the following equation:

17

$$\Phi_{DP} = \Phi_{HH} - \Phi_{VV} \tag{5}$$

where Φ_{HH} is the phase shift of the horizontally transmitted and received signal and Φ_{VV} is the phase shift of the vertically transmitted and received signal (Kumjian, 2013a; Rinehart, 2010). Φ_{DP}, however, does not reset along the radial direction so if the value increases by propagating through a rain shaft, it will maintain that degree of separation even after it has exited the rain shaft and is propagating through clear air. For this reason Φ_{DP} is not a useful tool in hydrometeor classifications. A more useful related product is specific differential phase (K_{DP}), which provides a measure of the amount of differential phase shift per unit distance (Kumjian, 2013a; Rinehart, 2010). It is measured in degrees per kilometer and is calculated by the following equation:

$$K_{DP} = \frac{\Phi_{DP}(r_2) - \Phi_{DP}(r_1)}{2(r_2 - r_1)} \tag{6}$$

where r_1 and r_2 are the two different ranges of interest along the beam path. K_{DP} is dependent on orientation, shape, size, number concentration and phase of the hydrometeors. Thus, K_{DP} values will be largest for heavy rain with large raindrops and will return near zero values for spherical hydrometeors, or hydrometeors like hail that appear spherical due to their chaotic tumbling nature (Kumjian, 2013a; Rinehart, 2010). K_{DP} values are often not displayed by the radar if there is too much noise in the radar data or the phase shift cannot be determined. When the beam propagates through light rain or non-Rayleigh scatters such as large hail, the radar has difficulty calculating a change in phase. The main application for the K_{DP} product is to locate areas of heavy precipitation. Therefore, if the radar beam propagates through areas that do not return water droplet

signatures, K_{DP} values will not be displayed. The consistency of hydrometeors within a pulse volume is determined by the DP product correlation coefficient (CC). CC is a unitless value that measures the similarity, or uniformity, of targets within each volume scan from one pulse to the next. This value is measured from 0 to 1, where the number 1 represents exact uniformity from pulse to pulse, and any number less than 0.8 indicates that the pulses vary too much from one pulse to the next to be considered meteorological targets. Targets with similar size and shape, like large raindrops, return CC values approaching 1. If the CC falls below 0.9, indicating the area consists of mixed hydrometeors or the raindrop concentration is low, K_{DP} will not displayed by the radar (Kumjian, 2013a; 2013c).

2.6 Dual-Polarization Studies of Lightning Initiation

Since the implementation of DP radar, meteorologist and hydrologist have been trying to determine what forecasting improvements can be developed using this new technology. One notable improvement associated with DP radar is the capability to distinguish between precipitation types due to their shape and orientation. This added capability allows forecasters to not only visualize the updraft through reflectivity cross-sections but also determine hydrometeor type within the updraft using DP products such as Z_{DR} (Kumjian 2013a; Rinehart, 2010). Studies of Z combined with Z_{DR} at specific thermal levels have mostly focused on hydrometeor classification but some researchers have discovered possible connections between Z combined with Z_{DR} values and CG lightning initiation. These connections have shown potential for lightning initiation

forecasting techniques to be developed. (Lund et al., 2009; Bringi et al., 1997; Carey and

Rutledge, 1996; 2000; Jameson et al., 1996; Goodman et al., 1988).

Two notable results from these studies were that Bringi et al. (1997) discovered

lightning initiation from a single storm six minutes after the Z_{DR} column disappeared,

while Lund et al. (2009) found lightning initiation occurred with a Z_{DR} column of 0.375-

1.623dB and Z values between 37.5-57.5dBZ during a small mesoscale convective

system in Oklahoma. Unfortunately, independent outcomes from case studies are not

robust enough to develop lightning initiation forecasting methods for an operational

setting.

This study builds upon previous studies and more recent research conducted by

Woodard (2011) in an effort to test forecasting methods using DP radar capabilities to

improve CG lightning initiation forecasting at CCAFS/KSC. Woodard (2011) analyzed

50 single-cell storms (31 lightning producing and 19 non-lightning producing) in

northern Alabama to determine if lightning initiation forecasting using conventional radar

(specifically the 40dBZ at -10°C threshold) could be improved using DP radar. It was

found that combining a Z_{DR} value of ≥ 1dB with Z values ≥ 40dBZ at -10°C produced a

lead time of 11 minutes for CG lightning initiation and reduced false alarm rates by 50%

compared to only using Z values ≥ 40dBZ at -10°C. Therefore this study was designed to

replicate and expand the forecasting techniques developed by Woodard (2011) by

analyzing single-cell thunderstorms over a new location, central Florida (CCAFS/KSC),

in the summer months of 2012 and 2013.

Research has identified the appearance of DP Z_{DR} signatures such as arcs,

tornadic debris, and columns within thunderstorms (Kumjian, 2013b). This study

examines the most notable of these signatures, the Z_{DR} column, defined as a region of

enhanced Z_{DR} values existing above the freezing level. These columns mark the location

of the updraft of a storm, where supercooled droplets and wet ice particles are lofted to

subfreezing temperatures while maintaining their mostly liquid state (Kumjian, 2013b).

Significant electrification through NIC in a developing thunderstorm will not begin until

glaciation of these drops occurs within the updraft. Thus, the detection of a Z_{DR} column

and subsequent disappearance of that column in a developing convective cell should

precede the onset of lightning (Kumjian, 2013b). Furthermore, decreasing Z_{DR} values

paired with increasing Z values within an updraft is indicative of imminent lightning

initiation. Z_{DR} values associated with a Z_{DR} column are typically greater than 1dB within

the column, which consist of mostly liquid hydrometeors, while Z_{DR} values less than 1dB

found outside of the column, consist of mostly frozen hydrometeors. A graphical

representation and more in depth details of Z_{DR} columns are given in the Warning

Decision Training Branch (2013) documentation and can be seen in Figure 5.
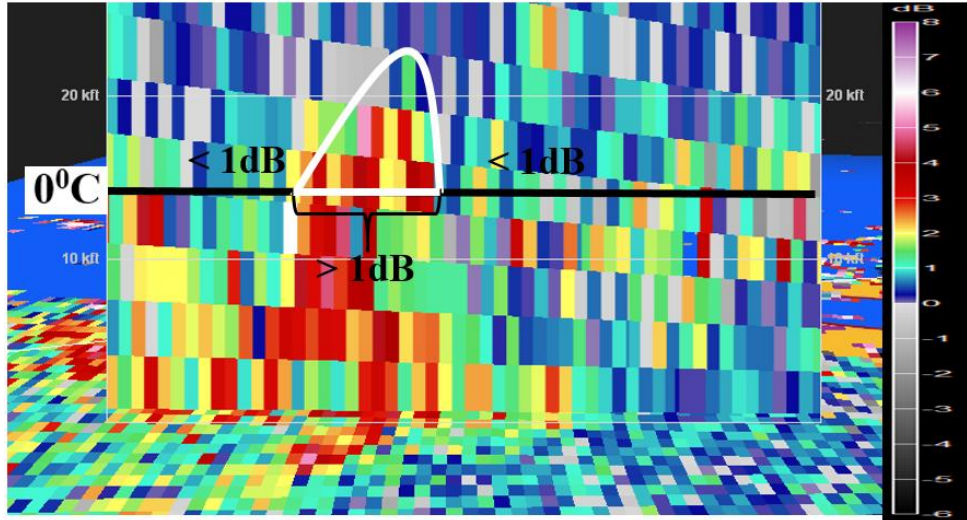
Figure 5: Z_{DR} column. A vertical cross-section of Z_{DR} column from a lightning producing storm near CCAFS/KSC on 7 September 2012. The bold horizontal black line represents the 0°C height and the white line indicates the area within the Z_{DR} column where values exceed 1dB above the freezing level, indicative of supercooled drops. The Z_{DR} values outside the column are typically less than 1dB.

This study analyzed Z_{DR} columns to find a useful updraft detection application to be used in CG lightning initiation forecasting. Since Z_{DR} columns are good indicators for supercooled raindrops, this study theorizes that K_{DP} values will be high in the same region of the storm's Z_{DR} column, creating a column of high K_{DP} values. Therefore this study makes the assumption that an updraft containing high concentrations of large supercooled droplets will produce a Z_{DR} column and high K_{DP} values on radar that can be coupled with Z values above the freezing level (ex: 40dBZ at -10°C) to test lightning initiation forecasting techniques. This is because mixed type hydrometeors in proximity is a necessary condition for thunderstorm charging, and it is believed that using the DP radar will allow for better and faster identification of supercooled droplet signatures. These signatures indicate the imminent formation of graupel and snow, and enable the ability to predict thunderstorm charging before CG lightning occurs.

III. Methodology

3.1 Thunderstorm Cell Selection

This research focused on single-cell thunderstorms near CCAFS/KSC formed during unstable conditions by convective processes discussed in the previous sections. Lightning produced by large synoptic systems such as fronts or squall lines was not evaluated. The same method implemented by Woodard (2011) was used to initially identify each thunderstorm for analysis. This involved using the Larson area method of radar analysis and lightning formation location (Larson and Stansbury, 1974). The Larson area is defined as a region of significant radar reflectivity at a specific thermal level. A Larson area with a horizontal reflectivity threshold of ≥ 30dBZ at -10° C was chosen as a baseline for thunderstorm development (Woodard et al., 2012; Woodard, 2011). The -10° C level marks the lowest level of the main charging zone where lightning formation and initiation is most common. A Z value ≥ 30dBZ at -10° C indicates an updraft strong enough to suspend hydrometeors such as supercooled drops, graupel, and ice crystals together, which enables thunderstorm electrification through NIC processes (Woodard, 2011). Dual-polarization parameters were evaluated for each volume scan between the time a cell exceeded the Larson area threshold and first CG lighting discharge. An idealized example of which volume scan elevation angle of the radar intersects the -10° C and -15° C thermal levels is shown in Figure 6. This figure depicts how the volume scan that intersects each thermal level changes based on the storm distance from the radar.
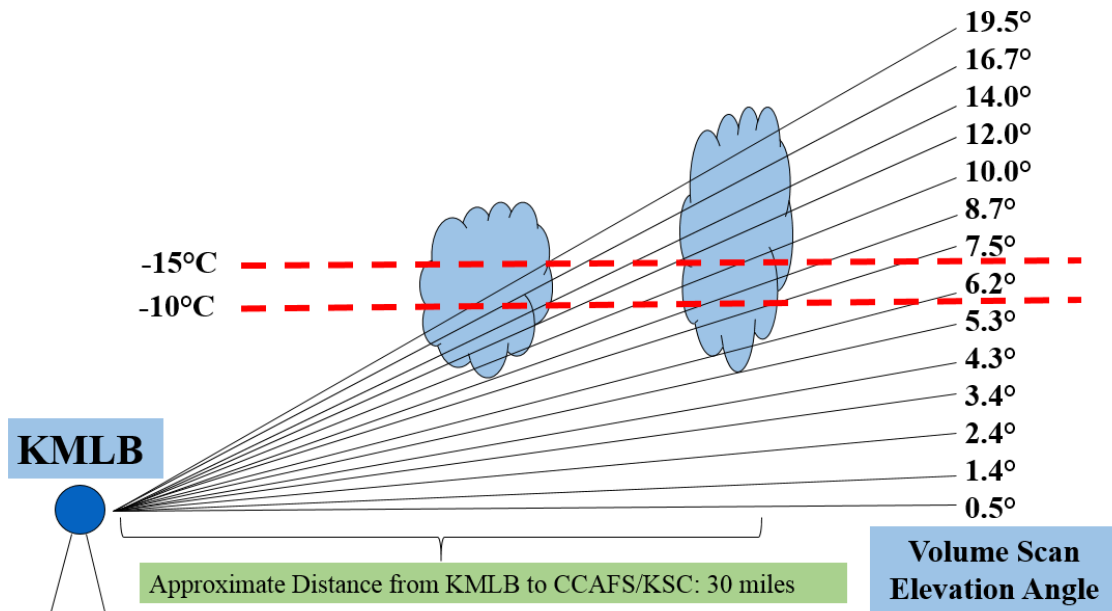
Figure 6: KMLB volume scans. An idealized depiction of the volume scan elevation angles of KMLB relative to CCAFS/KSC (approximately 30 miles). The red dashed lines represent the -10° and -15°C thermal levels. The elevation scan that intersects these thermal levels changes depending on the distance to the radar.

3.2 Data

The data needed for this study included atmospheric soundings, lightning and radar data. The timeframe covered in this study was from May to September 2012 and from May to July 2013, in order to focus on single-cell convective thunderstorms storms frequent in the summer months of Florida. The height of the -10°C and -15°C thermal levels, time and location of the first lightning occurrence, and radar volume scans leading up to lightning initiation were collected for each cell. Additionally, any volume scans that reached the Larson area threshold were recorded.

Atmospheric soundings are launched daily at the CCAFS Skid Strip (KXMR; WMO station number 74794) at 09 UTC (04 LST) and occasionally at 15 UTC (10 LST). These soundings were obtained from the University of Wyoming website (University of Wyoming, 2013).

Since single-cell convection typically initiates from surface heating in the afternoon, therefore the 15 UTC sounding was preferentially used to determine the height of the -10°C and -15°C thermal levels for each day studied. When the 15 UTC sounding was unavailable, the 09 UTC sounding was used. There is some inherent error in the height of the -10°C and -15°C thermal levels when using a sounding that may be several hours old, however, this error should be small compared to the radial beam width of 1° from KMLB which is approximately 500m at the distance of CCAFS/KSC.

CG lightning time and location were collected from the Marshall Space Flight Center website (MSFC) (Marshall Space Flight Center, 2013). An example of the interface used to obtain lightning data from this website is shown in Figure 7.
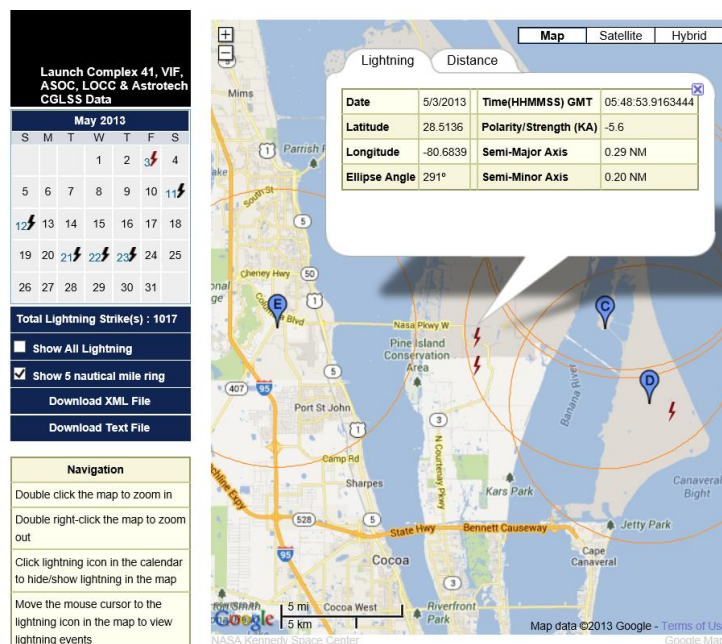
Figure 7: Lightning data from 03 May 2013 near CCAFS/KSC. The information for each CG lightning strike (red lightning bolt symbol) is shown if the cursor is positioned over it. The days that have archived CG lightning strikes are highlighted in blue with a lightning bolt symbol in the calendar on the top left. The range rings in which lightning data is archived are shown in orange circles of 5nmi radius. (Marshall Space Flight Center, 2013).

The MSFC website was used in conjunction with radar scans to determine if a cell produced lightning, and once produced, which thunderstorm cell produced the lightning in question.

Lastly, level-II radar data was downloaded from the Hierarchical Data Storage System (HDSS) Access System (HAS) (National Climatic Data Center 2013). The radar data was imported into the radar display program GR2Analyst Version 1.92b (GRLevelX, 2013) to visualize and manipulate the data.

3.3 Analysis

First, days where lightning occurred were identified using the MSFC website mentioned in the previous section. There were 32 days in which lightning was recorded within the range rings near CCAFS/KSC from May to September 2012, and 39 days from May to July 2013. The months of August and September 2013 were not archived in the MSFC website and therefore were not available for this study. All lightning strikes that occurred at night or from large clusters of cells such as fronts or squall lines were not analyzed. The cells were only analyzed if they were isolated single-cell storms in the daytime to which lighting could be unambiguously attributed. Additionally, non-lightning producing cells were analyzed as long as the Larson area criterion was met and there were no lightning strikes in the area. Cells were not included if they developed or moved too close to the radar or if any portion of the storm top was cut off or unavailable for analysis. Lastly, the cells were not analyzed if all or part of the cell was outside the range rings shown in the MSFC website image from Figure 7. Figure 8 depicts an example of a cell on radar matched with lightning data from the MSFC website. This figure shows that

there is limited uncertainty about where the lightning came from, since there is only one cell in the area. Figure 9 shows an example of storms that were not included in the study due to radar storm cell vs. lightning initiation uncertainty. The lightning strike in Figure 9a occurred too close to the edge of the range ring to be sure that it was the first lightning strike produced. There were also multiple cells in the area from which the lightning strike could have originated. Therefore this specific example and others like it were excluded from the study.

Over 200 lightning producing and non-lightning producing storms were analyzed, but only 68 storms met all the restrictive criteria required for inclusion in the study. Of these 68 convective cells, 44 produced lightning and 24 did not produce lightning. It was important to include a mixture of both lightning producing and non-lightning producing cells in order to determine both how well the DP techniques predicted the onset of lightning correctly and avoided falsely predicting lightning when it did not occur. The other primary metric evaluated was forecast lead time. For example, increasing the lead time of lightning onset compared to traditional reflectivity techniques while at least maintaining the same statistical skill. The selection process was strict to maintain certainty that the storms analyzed were single-cell convective storms in which the exact time of lightning initiation was known; or to confirm that a non-lightning producing cell never produced lighting.
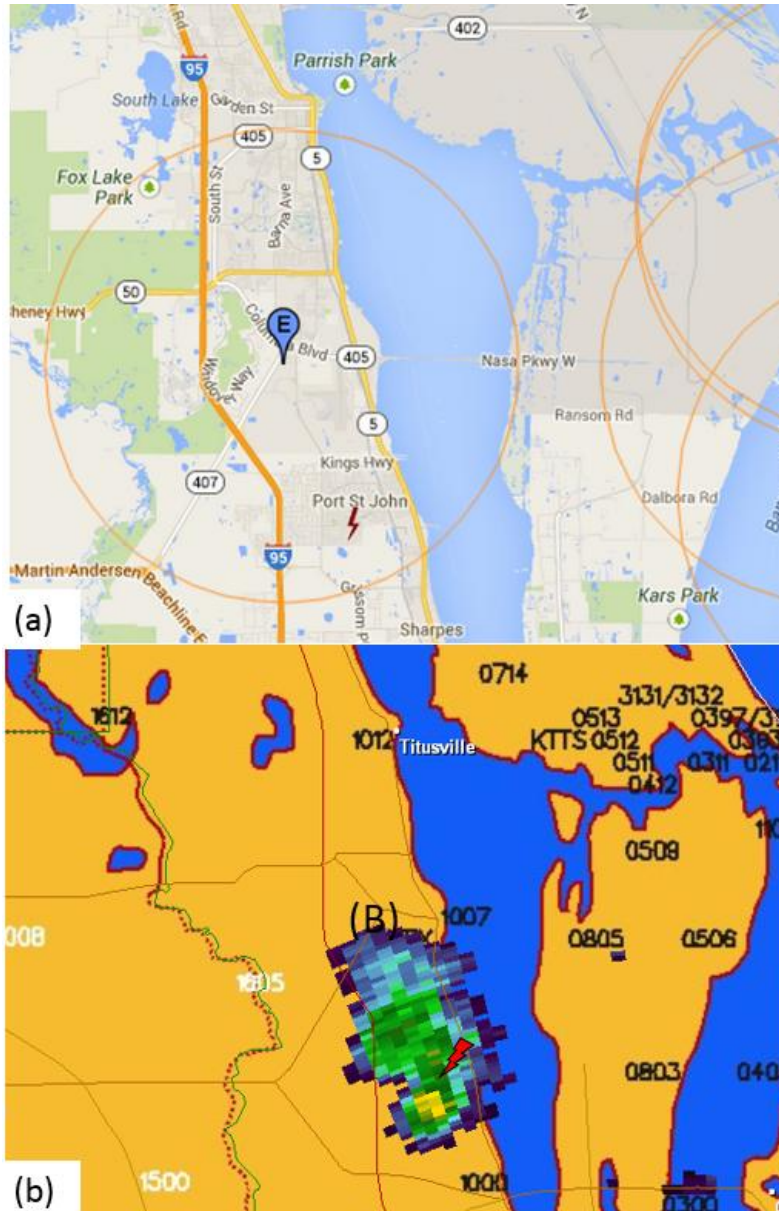
Figure 8: Good single-cell example. Image (a) shows the location of the initial lightning strike (23 June 2013 14:56:09 UTC) from the thunderstorm cell in image (b). Image (b) shows a base reflectivity radar image from KMLB over East-Central Florida on 23 June 2013, volume scan 10.0° (approximately at the -10°C height) at 14:58:48 UTC. The red lightning bolt represents the location of lightning initiation. (Marshall Space Flight Center, 2013).
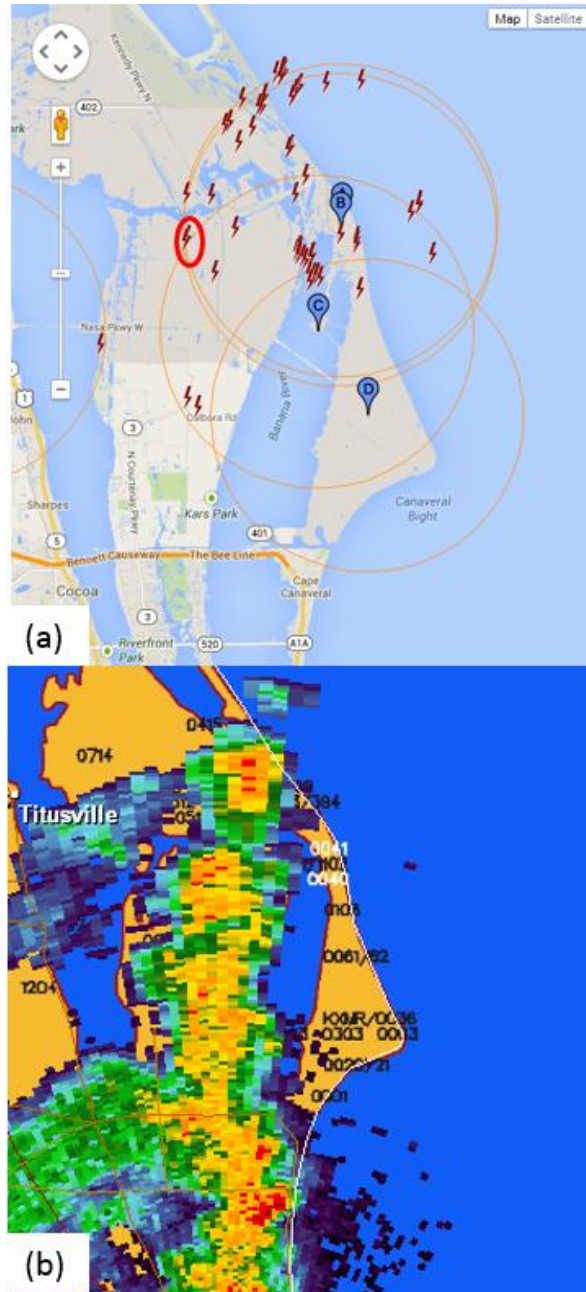
Figure 9: Bad single-cell example. Image (a) shows multiple lightning strikes produced from the storms in image (b). The red bold circle (a) shows a lightning strike that occurred at 20:57:13 on the edge of the range ring that cannot be analyzed with absolute certainty that it was the first lightning strike produced from a single storm. Image (b) shows a base reflectivity radar image from KMLB over East-Central Florida on 24 July 2012, volume scan 5.3° (approximately at the -10°C height) at 20:54:20 UTC. (Marshall Space Flight Center, 2013).

After an initial CG lightning strike was determined to originate from a specific single-cell storm, the cell was tracked backward in previous radar scans to investigate its development and record the maximum Z, Z_{DR}, and K_{DP} values at or above the -10°C and -15°C thermal levels. These cells were tracked back in time until they no longer met the Larson area criterion. For non-lighting producing storms, each volume scan's maximum Z, Z_{DR}, and K_{DP} values were also recorded while the Larson area was met. The GR2Analyst software enables user-selected elevation angles in a plan position indicator (PPI) view, radar beam height determination, radar parameter value, and exact mouse location using the cursor readout.
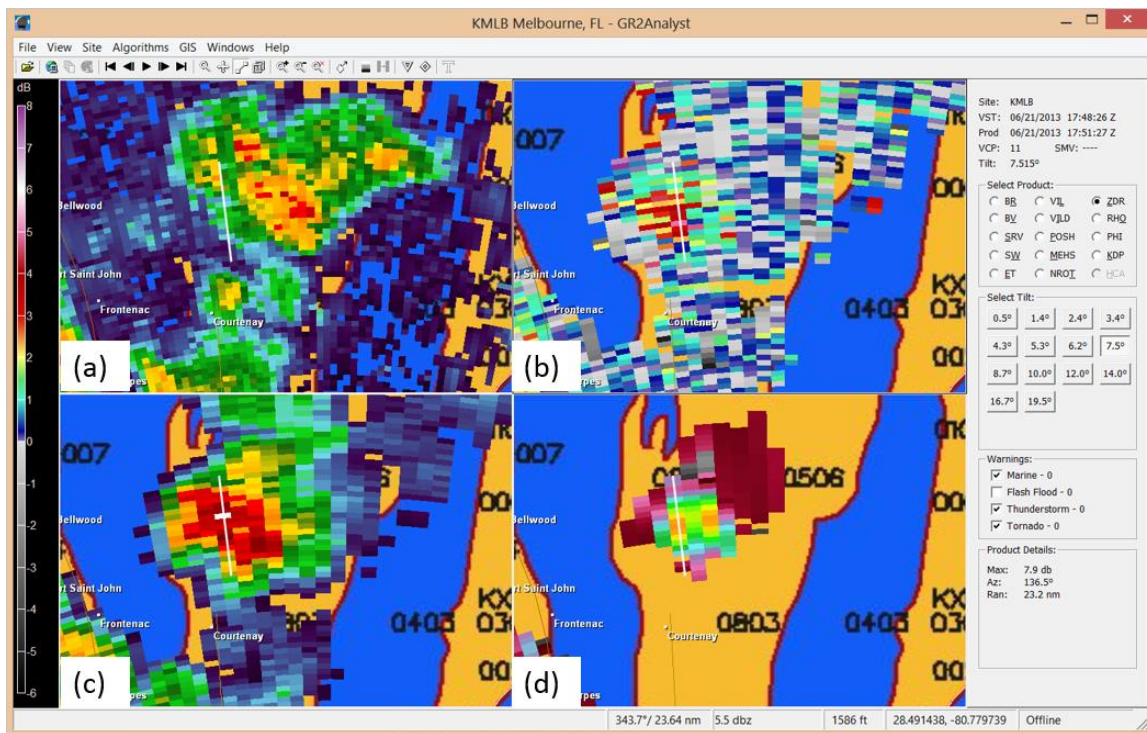
Figure 10: GR2Analyst display window. Image of the GR2Analyst PPI user display window of a lightning producing storm on 21 June 2013 near CCAFS/KSC using radar data from KMLB. Image (a) shows Z at 0.5° volume scan, image (b) shows Z_{DR} at 7.5° volume scan, image (c) shows Z at 7.5° volume scan, and image (d) shows K_{DP} at 7.5° volume scan. The white line represents the cross section analyzed shown in Figure 11.

30
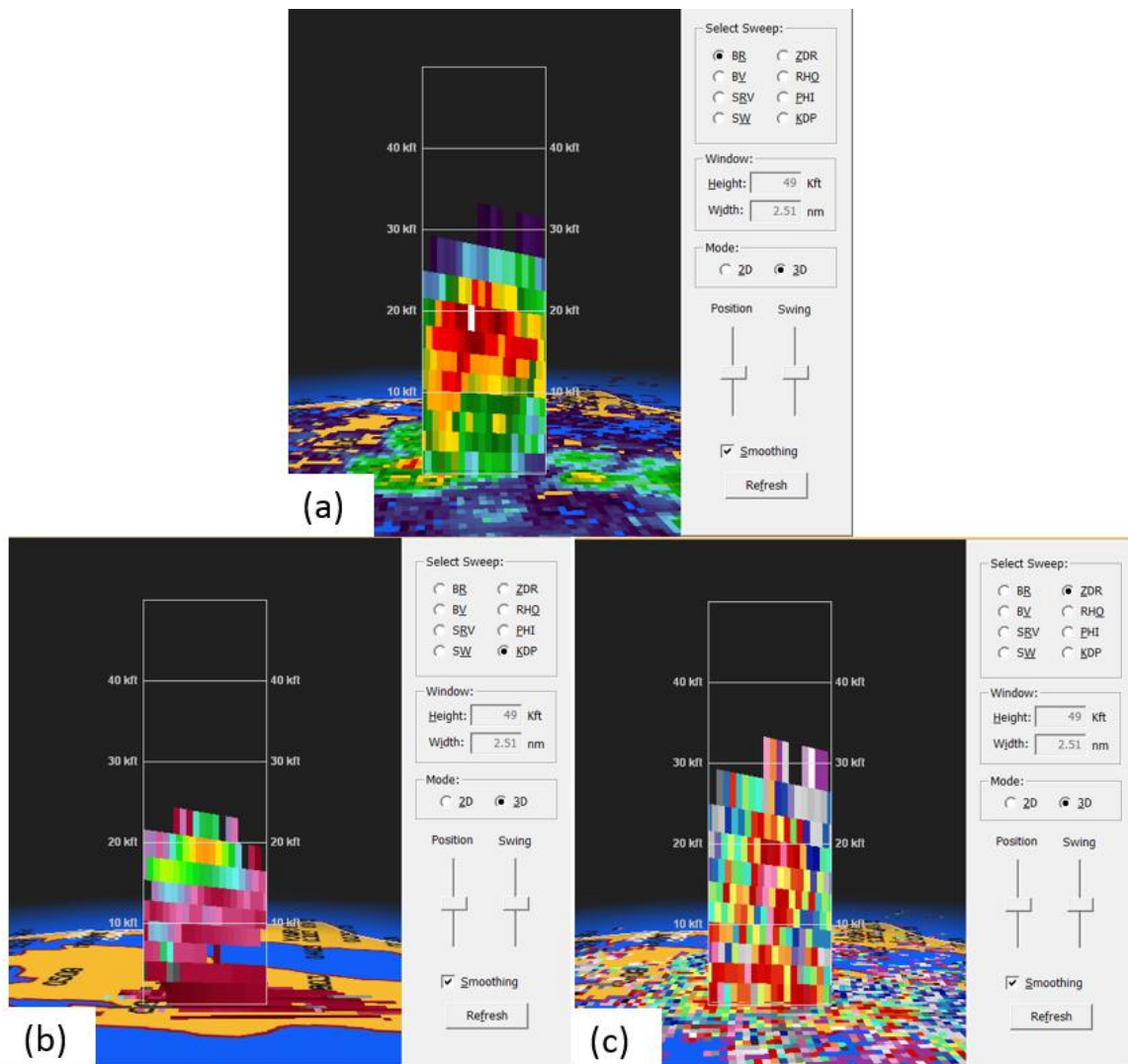
Figure 11: GR2Analyst cross section. Vertical cross section taken from a storm on 21 June 2013 using GR2Analyst for Z image (a), K_{DP} image (b), and Z_{DR} image (c).

Each of the 68 single-cell storms selected was interrogated using the GR2Analyst's

vertical cross section tool. Examples of storm cell interrogation are shown in Figures 10

and 11 for the lightning producing storm on 21 June 2013. This storm, like all other

lightning producing storms in this study, was analyzed from the moment of CG lightning

initiation backward in time to before the Larson area was met. The maximum Z, Z_{DR},

and K_{DP} values were recorded at the -10°C and -15°C heights using the GR2Analyst's

cursor readout function. Both lightning and non-lightning producing cells were analyzed to create a testable dataset of storms using statistical skill scores.

3.3.1 Training Data Set Z, Z_{DR}, and K_{DP} Values

The complete data set of 68 single-cell storms was split into two equal data sets of 34 storms each in order to develop a method to test lightning initiation techniques and validate it. The training data set consisted of 21 lightning producing storms and 13 non-lightning producing storms. The individual volume scans leading to lightning initiation of the 21 lightning producing storms were grouped into bins according to their time before lighting initiation. Bins were 2 minutes 30 seconds long from zero to 30 minutes prior to lightning and 5 minutes long from 30 to 50 minutes prior to lightning. Sample sizes ranged from 5 to 15 volume scans per time bin. The average and standard deviation of the maximum Z, Z_{DR}, and K_{DP} observed in each volume scan were calculated for each bin and are depicted in Figures 12a, 13a, and 14a. Volume scans for the 13 non-lightning producing were also arranged into 5 minute time bins with the highest Z value as the reference time. Average and standard deviations of the maximum Z, Z_{DR}, and K_{DP} for non-lightning producing storms are depicted in Figures 12b, 13b, and 14b. Figure 15 depicts the sample size in each time bin. Figures 12, 13, and 14 were used to determine typical ranges of Z, Z_{DR}, and K_{DP} for lightning producing and non-lightning producing storms. The results suggest that combinations of Z and Z_{DR} or Z and K_{DP} could be used to distinguish between lighting producing storms and non-lightning producing storms.
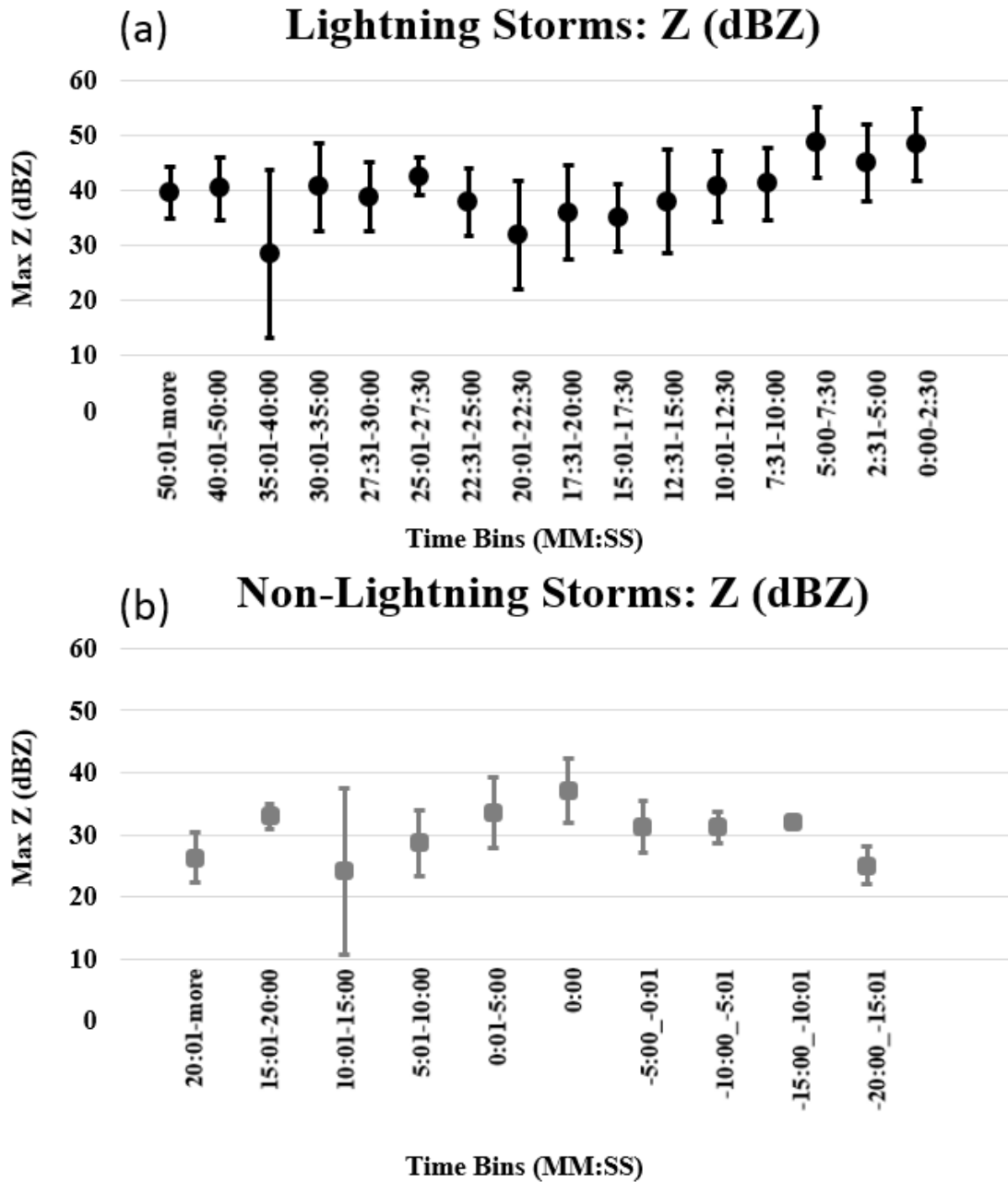
Figure 12: Reflectivity -10°C thermal level time bins. Plot of radar volume scans at -10°C height of 21 lightning producing single-cell thunderstorms leading up to lightning initiation at 0:00 min, organized into reflectivity time bins (a) and 13 non-lightning storms with maximum Z value occurring at 0:00 min organized into time bins (b). The marker (black dot for lightning storms (a) and grey square for non-lightning storms (b)) on each plot represents the average Z value for the time bin specified and the error bars represent the standard deviation.
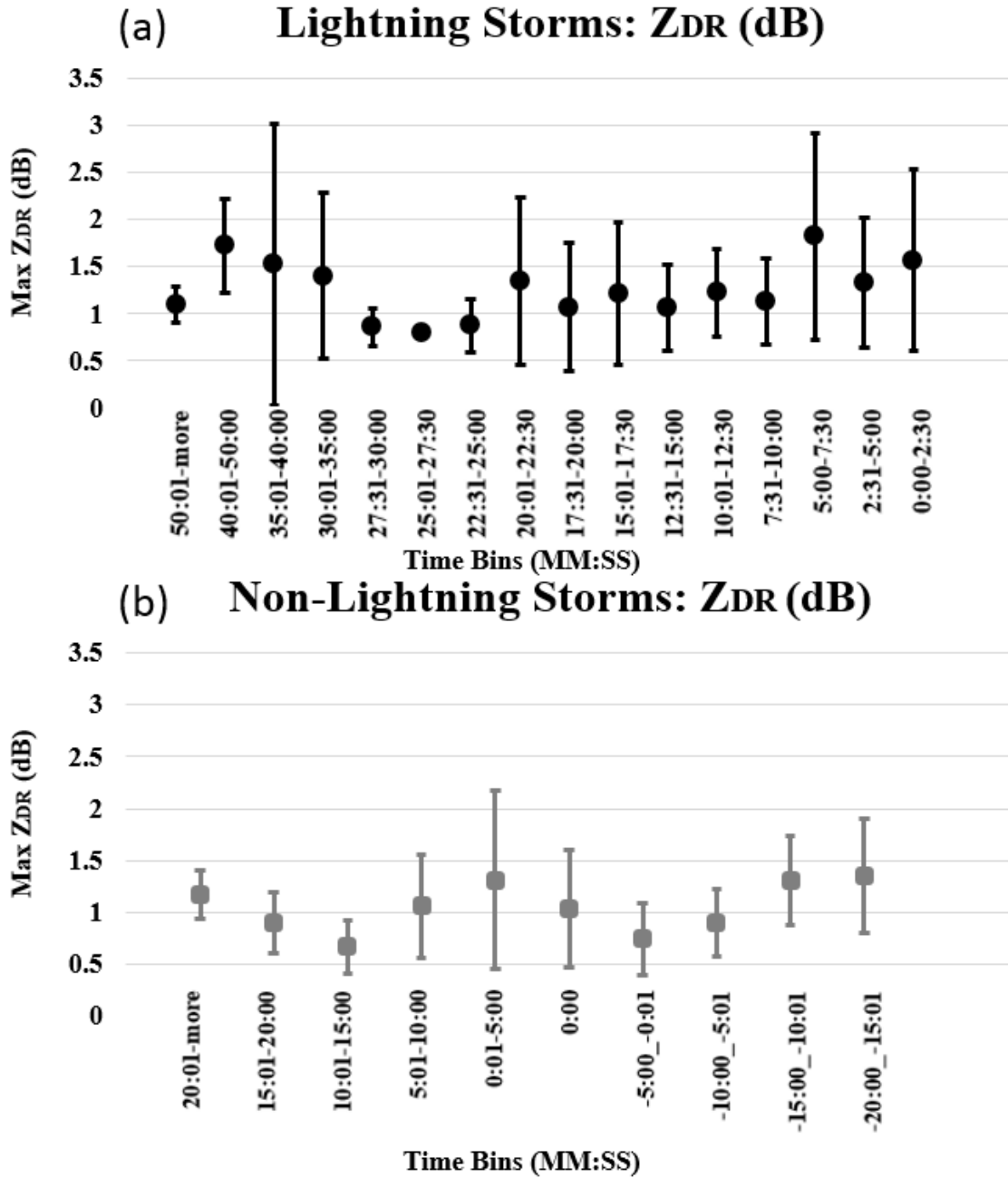
Figure 13: Differential reflectivity -10°C thermal level time bins. Plot of radar volume scans at -10°C height of 21 lightning producing single-cell thunderstorms leading up to lightning initiation at 0:00 min, organized into differential reflectivity time bins (a) and 13 non-lightning storms with maximum Z_{DR} values organized into time bins (b). The marker (black dot for lightning storms (a) and grey square for non-lightning storms (b)) on each plot represents the average Z_{DR} value for the time bin specified and the error bars represent the standard deviation.
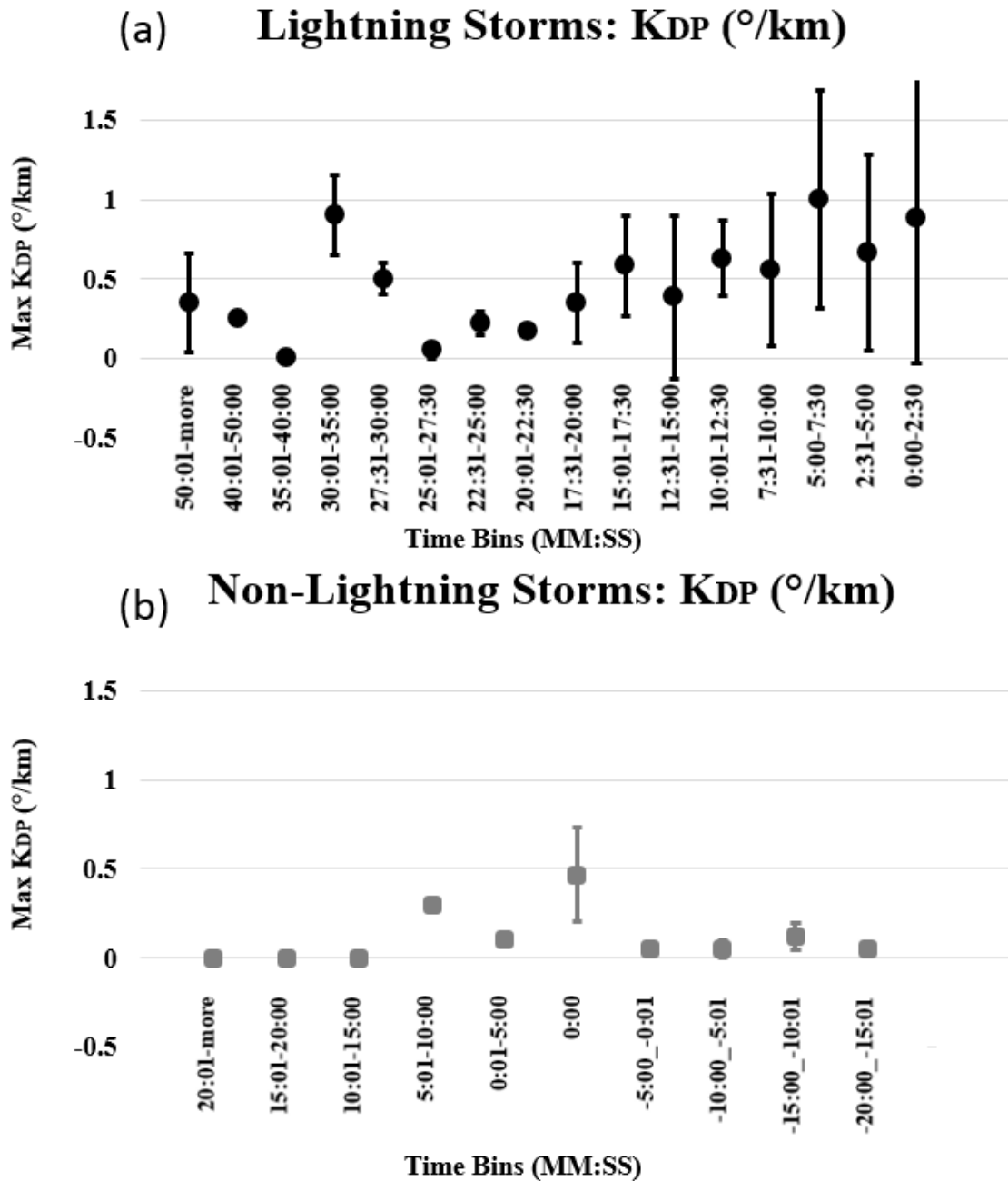
Figure 14: Specific differential phase -10°C thermal level time bins. Plot of radar volume scans at -10°C height of 21 lightning producing single-cell thunderstorms leading up to lightning initiation at 0:00 min, organized into specific differential phase time bins (a) and 13 non-lightning storms with maximum K_{DP} values organized into time bins (b). The marker (black dot for lightning storms (a) and grey square for non-lightning storms (b)) on each plot represents the average K_{DP} value for the time bin specified and the error bars represent the standard deviation.

(a) Lightning Storms: Number of Z, Z_DR, and K_DP Values Per Time Bin at -10 deg C

(b) Non-Lightning Storms: Number of Z, Z_DR, and K_DP Values Per Time Bin at -10°C
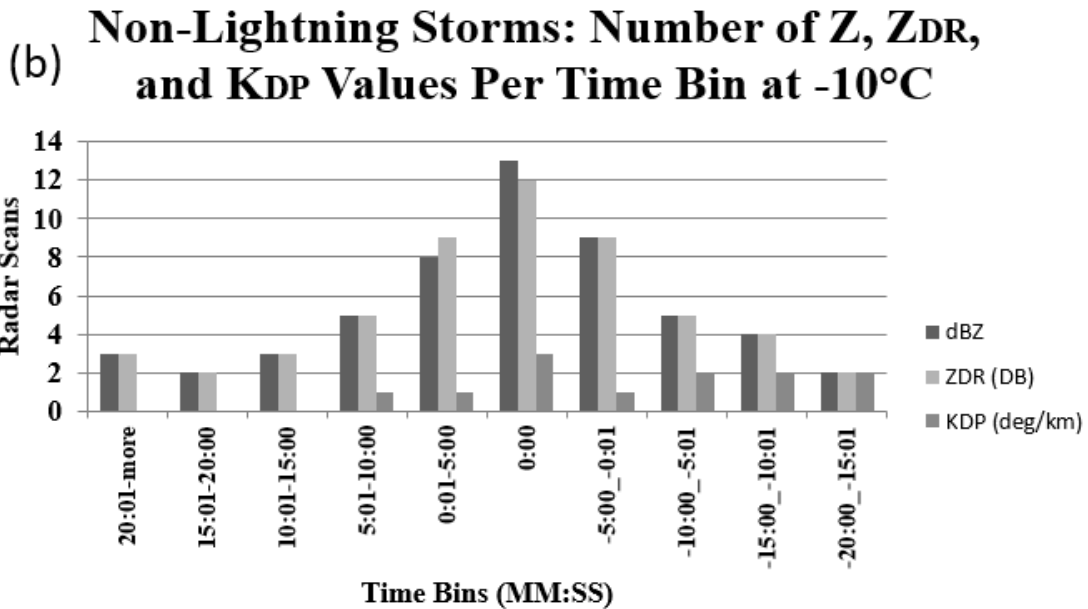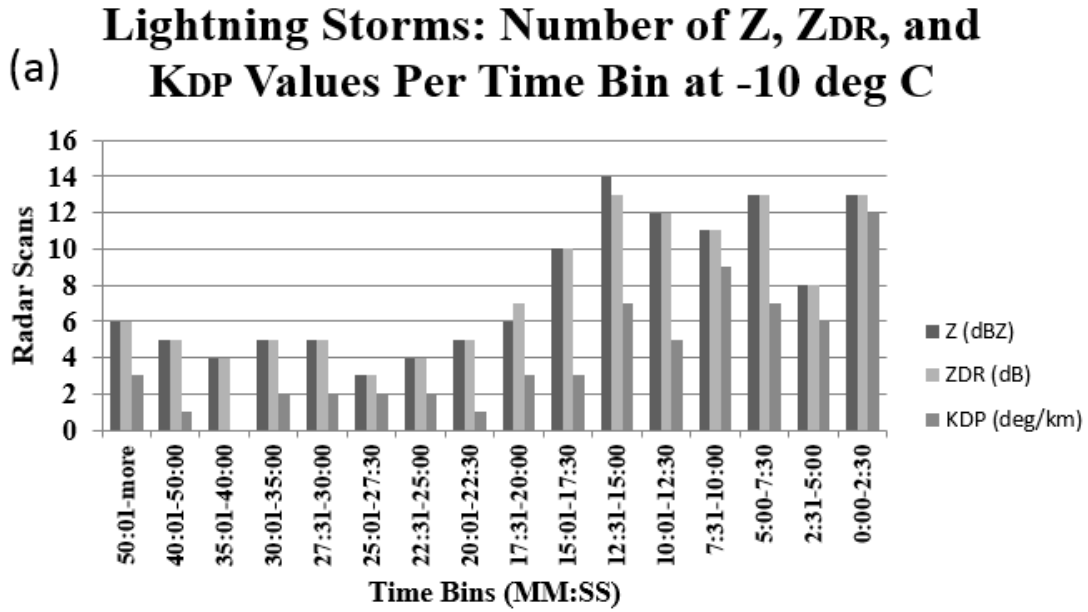
Figure 15: Number of volume scan data points per time bin. Plots of the number of values of reflectivity (Z), differential reflectivity (Z_{DR}), and specific differential phase (K_{DP}) for both lightning (a) and non-lightning (b) producing storms at the -10°C height used to create Figures 12, 13, and 14.

Typically, Z values greater than 40dBZ, Z_{DR} between 1 and 2dB, and K_{DP} larger than

0°/km were observed in lightning producing storms, while Z values less than 35dBZ, Z_{DR}

between 0.5 and 1.5dB, and K_{DP} near 0°/km were observed in non-lightning producing

storms. These ranges, along with the algorithm used in Woodard (2011), formed the

basis for the combined parameter thresholds tested on the validation data set.

3.3.2 Training Data Set Normalized Values

K_{DP} values are often unavailable, as seen in the low sample size in Figure 15. As

discussed in Chapter 2, when the CC value falls below 0.9 the K_{DP} value is not computed

(Kumjian, 2013a; 2013c). Due to the large number of volume scans with missing K_{DP}

values, a technique was developed to combine normalized Z, Z_{DR}, and K_{DP} values into a

single, averaged parameter. The mean and standard deviation for normalizing the

maximum Z, Z_{DR}, and K_{DP} values were calculated using every radar volume scan in the

training data set for lightning producing storms. These mean and standard deviation

values were calculated for both the -10°C and -15°C heights and are depicted in Table 2.

Table 2: Mean and standard deviation values of the training data set lightning producing
storms at -10°C and -15°C

-10°C Parameter	Mean	Standard Deviation
Max Z	37.753	9.606
Max Z_{DR}	1.213	0.737
Max K_{DP}	0.604	0.606
-15°C Parameter	Mean	Standard Deviation
Max Z	31.571	11.554
Max Z_{DR}	1.012	0.668
Max K_{DP}	0.482	0.621

Maximum Z, Z_{DR}, and K_{DP} values from the validation data set were normalized using the means and standard deviations from Table 2. The normalized Z, Z_{DR}, and K_{DP} values (when available) were averaged together to calculate a single unitless value for each volume scan. An example of this normalization technique is depicted in Table 3.

Table 3: Normalized value examples at -10°C

		Z	Z_{DR}	K_{DP}	Combined
Example 1	Raw Value	43.5	1.1	0.75	
	Normalized Value	0.598	-.0153	0.241	0.229
		Z	Z_{DR}	K_{DP}	Combined
Example 2	Raw Value	38.0	1.0	-	
	Normalized Value	0.026	-0.289	-	-0.132

This table shows two examples that represent two different radar volume scans with the maximum Z, Z_{DR}, and K_{DP} values observed at the -10°C thermal level. The normalized value for each parameter is shown below each variable. The combined value, which averages the available normalized values, represents the normalized average parameter for each volume scan. These calculations were determined for every volume scan of the validation data set. Total normalized values from 1 to -1 were tested individually at -10°C and -15°C for the third and final CG lightning initiation forecasting algorithm.

3.4 Forecast Verification (Skill Scores)

Various combined Z, Z_{DR}, and K_{DP} thresholds, as well as averaged normalized parameters, and Woodard's (2011) thresholds were tested on the validation data of 34 storms. Each algorithm was scored on both its average lead time before CG lightning and

a series of statistical skill scores. The skill scores used in this study include probability of detection (POD), probability of false alarm (PFA), false alarm ratio (FAR), true skill score (TSS), critical skill index (CSI), Heidke skill score (HSS), and operational utility index (OUI).

Skill scores are determined based on how well an algorithm performs statistically in forecasting the occurrence of an event (Jolliffe and Stephenson, 2003). Each event is categorized as a hit, miss, false alarm, or correct negative. The definitions of these outcomes are depicted in Table 4.

Table 4: Definitions of how an event's forecasts are categorized as a hit, miss, false alarm, or correct negative

Forecasted	Occurred	Category
Yes	Yes	Hit
No	Yes	Miss
Yes	No	False Alarm (FA)
No	No	Correct Negative (CN)

Each skill score used in this study is calculated based on a combination of two or more of the four possible categories for each event. Probability of detection (POD) is a commonly used meteorological statistic which gives the probability of an event being correctly forecast given that the event was observed. A POD of one is a perfect score (Jolliffe and Stephenson, 2003). POD is determined based on the number of hits and misses recorded for each case:

$$POD = \frac{Hit}{Hit + Miss} \tag{7}$$

False alarm ratio (FAR) is the proportion of forecast occurrences that did not actually occur. A FAR of zero is a perfect score (Jolliffe and Stephenson, 2003). FAR is determined based on the number of hits and false alarms recorded for each case:

$$FAR = \frac{FA}{Hit + FA} \tag{8}$$

Probability of false alarm (PFA), often referred to as the probability of false detection (POFD), is defined as the fraction of non-occurrences in which a false alarm occurred. A PFA of zero is a perfect score (Barnes et al., 2009; Jolliffe and Stephenson, 2003). PFA is determined based on the number of false alarms and correct negatives recorded for each case:

$$PFA = \frac{FA}{FA + CN} \tag{9}$$

True skill score (TSS) is used to determine how well an algorithm case performs at predicting the occurrence of an event. TSS has a range of negative one to positive one where a TSS of zero would indicate no skill. A TSS of one is a perfect score. A negative one value indicates the case was a perfect predictor for determining the occurrence of non-thunderstorms (Jolliffe and Stephenson, 2003). TSS is determined based on the number of hits, misses, false alarms, and correct negatives recorded for each case:

$$TSS = \frac{(Hit * CN) - (FA * Miss)}{(Hit + Miss) * (FA + CN)} \tag{10}$$

Critical success index (CSI) is an estimate of the conditional probability of a hit given that the event was either forecast, observed, or both. A CSI of one is a perfect score (Jolliffe and Stephenson, 2003). CSI is determined based on the number of hits, misses, and false alarms recorded for each case:

$$CSI = \frac{Hit}{Hit + Miss + FA} \tag{11}$$

Heidke skill score (HSS) is a skill corrected verification measure of categorical forecast

performance which takes into account the number of hits due to chance. It calculates the

difference between correctly forecasted events and the total (observed and non-observed)

forecasted. A HSS of one is a perfect score (Jolliffe and Stephenson, 2003). HSS is

determined based on the number of hits, correct negatives, false alarms, and misses recorded

for each case:

$$HSS = \frac{[2\{(Hit * CN) - (FA * Miss)\}]}{[(Hit + Miss)(Miss + CN) + (Hit + FA)(FA + CN)]} \tag{12}$$

Operational utility index (OUI) was developed and is used by the 45 WS to optimize

lightning prediction techniques for their operations at CCAFS/KSC. The OUI is a non-

standard performance metric that combines POD, FAR, and TSS to represent the

operational priorities of 45 WS. OUI gives a weight of three to POD because of the

importance of personnel safety, a weight of two to TSS since skill is also important, and a

lower weight of one to FAR since 45 WS is willing to have a small increase in false

alarms in lightning warning to get higher POD. The ideal score for this skill is 0.83 and

an unacceptable score is less than or equal to zero (Woodard, 2011; D'Archangelo,

2000).

$$OUI = \frac{[(3 * POD) + (2 * TSS) + (-1 * FAR)]}{6} \tag{13}$$

41

IV. Results

This study followed similar research by Woodard (2011) in an effort to test the benefits of using DP radar over conventional radar to forecast lightning initiation. In this study, single-cell convective lightning producing and non-lightning producing storms that met the Larson area criteria were analyzed near CCAFS/KSC. The goal was to compare DP radar capabilities to a standard lightning initiation technique of $Z \geq 40dBZ$ at -10°C. 68 single-cell storms were evaluated and the data set was split into a training and validation data set of equal size (34 storms each). The training data set discussed in Chapter 3, was used to develop lightning initiation techniques to test on the validation data set. The validation data set consisted of 23 lighting producing and 11 non-lightning producing storms. This chapter will discuss the results of the standard lightning initiation technique along with variations of this technique. Additionally, results from three DP radar algorithms developed through the training data set will be discussed. The three DP radar algorithms tested in this study were Z combined with Z_{DR} at -10°C and -15°C, Z combined with K_{DP} at -10°C and -15°C, and an averaged normalized value of Z, Z_{DR}, and K_{DP} at -10°C and -15°C.

4.1 Standard Forecasting Technique ($Z \geq 40dBZ$ at -10°C)

Previous research (Yang and King, 2010; Wolf, 2006; Vincent et al., 2003; Gremillion and Orville, 1999; Buechler and Goodman, 1990; Dye et al., 1989) concluded that observing $Z \geq 40dBZ$ at -10°C produced the best results in forecasting CG lightning initiation. This technique was used as the standard to compare against additional forecasting techniques/algorithms to determine if they improved the standard. When this

standard case was applied to the 34 storms of the validation data, the forecast resulted in

22 hits, 1 miss, 7 false alarms, and 4 correct negatives. This produced a high POD of

0.957 and moderate results for the remaining skill scores with an average lead time of 14

minutes 33 seconds. These results were similar to those observed by Woodard (2011) as

shown in Table 5. Although the results differ slightly there is reasonable agreement

between the two, given they were generated over different geographical areas.

Table 5: Standard case ($Z \geq 40dBZ$ at -10°C) results of this research (2014) compared to
Woodard (2011)

Standard Case	POD	FAR	PFA	TSS	CSI	HSS	OUI	Avg Lead Time
Researcher 2014	0.957	0.241	0.636	0.320	0.733	0.373	0.545	0:14:33
Woodard 2011	1.000	0.308	0.522	0.478	0.692	0.497	0.608	0:14:00

4.2 Reflectivity Cases at -10^{0}C and -15°C

The first forecasting technique tested on the validation data combined different

values of Z at both -10°C and -15°C thermal heights. The results of the different cases

tested were compared to the standard and are shown in Table 6 while the skill scores and

average lead times are shown in Table 7.

The Z values tested at -10°C included 45dBZ, 40dBZ, and 35dBZ. Although the

standard case proved to be better than the 45dBZ at -10°C, the 35dBZ at -10°C case

produced the best results with a perfect POD, slightly better FAR, TSS, CSI, HSS, OUI,

and an increased average lead time of 2 minutes 14 seconds.

Table 6: Forecasting results for conventional radar cases with the standard bolded

Case	Hit	Miss	FA	CN
40dBZ -10°C	**22**	**1**	**7**	**4**
45dBZ -10°C	18	5	7	4
35dBZ -10°C	23	0	7	4
40dBZ -15°C	17	6	0	11
35dBZ -15°C	*23*	*0*	*1*	*10*
30dBZ -15°C	23	0	6	5

Table 7: Skill score and lead time results for conventional radar cases with the standard bolded

Case	POD	FAR	PFA	TSS	CSI	HSS	OUI	Avg Lead Time
40dBZ -10°C	**0.957**	**0.241**	**0.636**	**0.320**	**0.733**	**0.373**	**0.545**	**0:14:33**
45dBZ -10°C	0.783	0.280	0.636	0.146	0.600	0.154	0.393	0:12:12
35dBZ -10°C	1.000	0.233	0.636	0.364	0.767	0.436	0.582	0:16:47
40dBZ -15°C	0.739	0.000	0.000	0.739	0.739	0.647	0.616	0:08:27
35dBZ -15°C	*1.000*	*0.042*	*0.091*	*0.909*	*0.958*	*0.931*	*0.796*	*0:09:46*
30dBZ -15°C	1.000	0.207	0.545	0.455	0.793	0.530	0.617	0:13:47

The best statistical results of the six conventional radar cases tested, however, came from the 35dBZ at -15°C, italicized in Tables 6 and 7. This case allowed for no misses and only 1 false alarm, producing a perfect POD and improving every other skill score tested when compared to the standard. This case also improved every skill score tested compared to all six cases, with the two exceptions of FAR and PFA when compared to 40dBZ at -15°C. The flaw of this case was that it reduced the average lead time by 4 minutes 47 seconds. Depending on the operational user, a decrease in lead time of nearly 5 minutes might be unacceptable. Therefore the 35dBZ at -15C improved skill scores

over the standard would not be enough to warrant a change in current operational

forecasting methods.

4.3 Combined Z and Z_{DR} Algorithm Cases at -10°C and -15°C

Z_{DR} was used in conjunction with Z at -10°C and -15°C to test CG lightning

initiation forecast techniques against the standard. These values were determined from

both previous research by Woodard (2011) and the training data set. The forecast results

of these cases are shown in Table 8 while the skill scores and average lead times are

depicted in Table 9.

Table 8: Forecasting results for Z and Z_{DR} algorithm cases with the standard bolded

Case	Hit	Miss	FA	CN
40dBZ -10°C	**22**	**1**	**7**	**4**
40dBZ&1.5dB -10°C	19	4	7	4
40dBZ&1.0dB -10°C	22	1	7	4
40dBZ&0.5dB -10°C	22	1	7	4
35dBZ&1.5dB -10°C	19	4	7	4
35dBZ&1.0dB -10°C	*22*	*1*	*7*	*4*
35dBZ&0.5dB -10°C	23	0	7	4
30dBZ&1.5dB -10°C	19	4	7	4
30dBZ&1.0dB -10°C	*22*	*1*	*7*	*4*
30dBZ&0.5dB -10°C	*23*	*0*	*7*	*4*
35dBZ&1.5dB -15°C	13	10	0	11
35dBZ&1.0dB -15°C	18	5	0	11
35dBZ&0.5dB -15°C	*23*	*0*	*0*	*11*
30dBZ&1.5dB -15°C	13	10	0	11
30dBZ&1.0dB -15°C	20	3	3	8
30dBZ&0.5dB -15°C	*23*	*0*	*5*	*6*
25dBZ&1.5dB -15°C	13	10	1	10
25dBZ&1.0dB -15°C	20	3	5	6
25dBZ&0.5dB -15°C	23	0	7	4

Table 9: Skill score and lead time results for Z and Z_{DR} algorithm cases with the standard bolded

Case	POD	FAR	PFA	TSS	CSI	HSS	OUI	Avg Lead Time
40dBZ -10°C	**0.957**	**0.241**	**0.636**	**0.320**	**0.733**	**0.373**	**0.545**	**0:14:33**
40dBZ&1.5dB -10°C	0.826	0.269	0.636	0.190	0.633	0.204	0.431	0:13:27
40dBZ&1.0dB -10°C	0.957	0.241	0.636	0.320	0.733	0.373	0.545	0:13:55
40dBZ&0.5dB -10°C	0.957	0.241	0.636	0.320	0.733	0.373	0.545	0:14:33
35dBZ&1.5dB -10°C	0.826	0.269	0.636	0.190	0.633	0.204	0.431	0:14:27
35dBZ&1.0dB -10°C	*0.957*	*0.241*	*0.636*	*0.320*	*0.733*	*0.373*	*0.545*	*0:16:10*
35dBZ&0.5dB -10°C	1.0°0	0.233	0.636	0.364	0.767	0.436	0.582	0:16:47
30dBZ&1.5dB -10°C	0.826	0.269	0.636	0.190	0.633	0.204	0.431	0:15:51
30dBZ&1.0dB -10°C	*0.957*	*0.241*	*0.636*	*0.320*	*0.733*	*0.373*	*0.545*	*0:19:25*
30dBZ&0.5dB -10°C	*1.000*	*0.233*	*0.636*	*0.364*	*0.767*	*0.436*	*0.582*	*0:19:30*
35dBZ&1.5dB -15°C	0.565	0.000	0.000	0.565	0.565	0.457	0.417	0:11:56
35dBZ&1.0dB -15°C	0.783	0.000	0.000	0.783	0.783	0.700	0.652	0:10:30
35dBZ&0.5dB -15°C	*1.000*	*0.000*	*0.000*	*1.000*	*1.000*	*1.000*	*0.833*	*0:09:46*
30dBZ&1.5dB -15°C	0.565	0.000	0.000	0.565	0.565	0.457	0.471	0:14:06
30dBZ&1.0dB -15°C	0.87	0.130	0.273	0.597	0.769	0.597	0.612	0:13:04
30dBZ&0.5dB -15°C	*1.000*	*0.179*	*0.455*	*0.545*	*0.821*	*0.619*	*0.652*	*0:13:33*
25dBZ&1.5dB -15°C	0.565	0.071	0.091	0.474	0.542	0.391	0.429	0:15:07
25dBZ&1.0dB -15°C	0.870	0.200	0.455	0.415	0.714	0.436	0.540	0:14:26
25dBZ&0.5dB -15°C	1.000	0.233	0.636	0.364	0.767	0.436	0.582	0:15:52

The research performed by Woodard (2011) tested cases that combined $Z_{DR} \geq$ 0.5dB, 1dB, and 4dB, $Z \geq 40$dBZ, and thermal heights of -10°C, -15°C, and -20°C. It was determined in their research that the best case was $Z \geq 40$dBZ combined with $Z_{DR} \geq$ 1dB at -10°C. This case slightly reduced POD, but improved PFA, FAR, TSS, CSI, HSS, and OUI, while adding 50 seconds to the standard. This current study did not duplicate Woodard's (2011) results. The 40dBZ and 1dB at -10°C case produced the exact forecasting results as the standard, with the same skill scores, yet decreased lead time by 38 seconds, adding no benefit to an operational user in Florida.

The 35dBZ and 0.5dB at -15°C case, italicized in Tables 8 and 9, produced the best statistical forecasting and skill score results in this study. This case produced 23 hits, 0 misses, 0 false alarms, and 11 correct negatives, which resulted in perfect skill scores for POD, FAR, PFA, TSS, CSI, HSS, and OUI. Although this case produced the best skill scores, it also reduced the average lead time by 4 minutes 47 seconds compared to the standard. This was the same reduction in average lead time produced by the 35dBZ at -15°C case, therefore, it would be up to the operational user to decide if having perfect skill scores would be worth decreasing the average lead time. The second best statistical case was 30dBZ and 0.5dB at -15°C. This case produced a perfect POD, a low FAR and PFA, and high TSS, CSI, HSS, and OUI when compared to the standard, but it also reduced the average lead time by 1 minute.

If the operational user determines the average lead time to be of equal weight or more important than skill scores, both the 35dBZ and 1dB at -10°C and the 30dBZ and 1dB at -10°C cases would be preferred. These cases produced identical statistical results to the standard but increased the average lead time by 1 min. 37 sec. and 4 min. 52 sec. respectively. Additionally, the three cases of 35dBZ and 0.5dB at -10°C, 30dBZ and 0.5dB at -10°C, and the 25dBZ and 0.5dB at -15°C all increased average lead time over the standard by 2 min. 14 sec., 4 min. 57 sec., and 1 min. 18 sec. respectively, while improving the skill scores. The skill scores of these three cases were exactly the same, therefore, the case which increased average lead time the most, 30dBZ and 0.5dB at -10°C, would be the best case if an increased lead time was desired most.

4.4 Combined Z and K$_{DP}$ Algorithm Cases at -10°C and -15°C

K$_{DP}$ was used in conjunction with Z at -10°C and -15°C to test additional DP radar CG lightning initiation forecasting techniques against the standard. The values tested were determined from the training data set. The forecasting results of these cases are depicted in Table 10 while the skill scores and average lead time results are depicted in Table 11.

Table 10: Forecasting results for Z and K$_{DP}$ algorithm cases with the standard bolded

Case	Hit	Miss	FA	CN
40dBZ -10°C	**22**	**1**	**7**	**4**
40dBZ&0.75°/km -10°C	4	19	0	11
40dBZ&0.5°/km -10°C	8	15	0	11
40dBZ&0.25°/km -10°C	12	11	0	11
40dBZ&0.1°/km -10°C	13	10	0	11
35dBZ&0.75°/km -10°C	5	18	0	11
35dBZ&0.5°/km -10°C	9	14	0	11
35dBZ&0.25°/km -10°C	15	8	0	11
35dBZ&0.1°/km -10°C	17	6	0	11
30dBZ&0.75°/km -10°C	5	18	0	11
30dBZ&0.5°/km -10°C	9	14	0	11
30dBZ&0.25°/km -10°C	15	8	0	11
30dBZ&0.1°/km -10°C	17	6	1	10
35dBZ&0.5°/km -15°C	9	14	0	11
35dBZ&0.25°/km -15°C	15	8	0	11
35dBZ&0.1°/km -15°C	17	6	0	11
30dBZ&0.5°/km -15°C	9	14	0	11
30dBZ&0.25°/km -15°C	15	8	0	11
30dBZ&0.1°/km -15°C	17	6	1	10
25dBZ&0.5°/km -15°C	9	14	0	11
25dBZ&0.25°/km -15°C	15	8	0	11
25dBZ&0.1°/km -15°C	17	6	2	9

Table 11: Skill score and lead time results for Z and K_{DP} algorithm cases with the standard bolded

Case	POD	FAR	PFA	TSS	CSI	HSS	OUI	Avg Lead Time
40dBZ -10°C	**0.957**	**0.241**	**0.636**	**0.320**	**0.733**	**0.373**	**0.545**	**0:14:33**
40dBZ&0.75°/km -10°C	0.174	0.000	0.000	0.174	0.174	0.120	0.145	0:03:49
40dBZ&0.5°/km -10°C	0.348	0.000	0.000	0.348	0.348	0.257	0.290	0:06:56
40dBZ&0.25°/km -10°C	0.522	0.000	0.000	0.522	0.522	0.414	0.435	0:07:17
40dBZ&0.1°/km -10°C	0.565	0.000	0.000	0.565	0.565	0.457	0.471	0:07:02
35dBZ&0.75°/km -10°C	0.217	0.000	0.000	0.217	0.217	0.152	0.181	0:03:28
35dBZ&0.5°/km -10°C	0.391	0.000	0.000	0.391	0.391	0.294	0.326	0:06:24
35dBZ&0.25°/km -10°C	0.652	0.000	0.000	0.652	0.652	0.548	0.543	0:06:33
35dBZ&0.1°/km -10°C	0.739	0.000	0.000	0.739	0.739	0.647	0.616	0:07:19
30dBZ&0.75°/km -10°C	0.217	0.000	0.000	0.217	0.217	0.152	0.181	0:03:28
30dBZ&0.5°/km -10°C	0.391	0.000	0.000	0.391	0.391	0.294	0.326	0:06:24
30dBZ&0.25°/km -10°C	0.652	0.000	0.000	0.652	0.652	0.548	0.543	0:06:49
30dBZ&0.1°/km -10°C	0.739	0.056	0.091	0.648	0.708	0.580	0.576	0:08:08
35dBZ&0.5°/km -15°C	0.391	0.000	0.000	0.391	0.391	0.294	0.326	0:06:24
35dBZ&0.25°/km -15°C	0.652	0.000	0.000	0.652	0.652	0.548	0.543	0:06:33
35dBZ&0.1°/km -15°C	0.739	0.000	0.000	0.739	0.739	0.647	0.616	0:07:19
30dBZ&0.5°/km -15°C	0.391	0.000	0.000	0.391	0.391	0.294	0.326	0:06:24
30dBZ&0.25°/km -15°C	0.652	0.000	0.000	0.652	0.652	0.548	0.543	0:06:49
30dBZ&0.1°/km -15°C	0.739	0.056	0.091	0.648	0.708	0.580	0.576	0:08:08
25dBZ&0.5°/km -15°C	0.391	0.000	0.000	0.391	0.391	0.294	0.326	0:06:24
25dBZ&0.25°/km -15°C	0.652	0.000	0.000	0.652	0.652	0.548	0.543	0:07:23
25dBZ&0.1°/km -15°C	0.739	0.105	0.182	0.557	0.68	0.509	0.538	0:09:34

It is apparent that some cases produced better individual skill scores than the standard case, yet no case improved POD or average lead time. Additionally no case improved the standard when all the skill scores and average lead time were evaluated together. Therefore an algorithm that consists of only Z and K_{DP} provided no benefit in CG lightning initiation forecasting over Florida.

4.5 Normalized Z, Z_{DR}, and K_{DP} Algorithm Cases at -10°C and -15°C

Although the K_{DP} algorithm tested did not improve upon the standard, it was believed that this product would still be useful in a third algorithm that included Z, Z_{DR}, and K_{DP} values at -10°C and -15°C. This final algorithm, as discussed in Chapter 3, used a normalized average parameter for each volume scan in the validation data. Multiple normalized values between 1 to -1 were tested to determine the best forecasting case for this algorithm. The forecasting results of these cases are shown in Table 12 while the skill scores and average lead times are shown in Table 13.

Table 12: Forecasting results for normalized Z, Z_{DR}, and K_{DP} algorithm cases with the standard bolded

Cases at -10°C	Hit	Miss	FA	CN
40dBZ -10°C	**20**	**3**	**3**	**8**
Normal: 0.25	20	3	3	8
Normal: 0.20	21	2	3	8
Normal: 0.15	21	2	3	8
Normal: 0.00	22	1	3	5
Normal: -0.05	*22*	*1*	*6*	*5*
Normal: -0.10	22	1	6	5
Normal: -0.15	22	1	7	4
Normal: -0.50	*23*	*0*	*8*	*3*

Cases at -15°C	Hit	Miss	FA	CN
Normal: 0.25	20	3	2	9
Normal: 0.15	20	3	2	9
Normal: 0.00	21	2	4	7
Normal: -0.05	21	2	4	7
Normal: -0.10	*23*	*0*	*4*	*7*
Normal: -0.20	*23*	*0*	*4*	*7*
Normal: -0.25	*23*	*0*	*4*	*7*

Table 13: Skill score and lead time results for normalized Z, Z_{DR}, and K_{DP} algorithm cases with the standard bolded

Cases at -10°C	POD	FAR	PFA	TSS	CSI	HSS	OUI	Avg Lead Time
40dBZ -10°C	**0.957**	**0.241**	**0.636**	**0.320**	**0.733**	**0.373**	**0.545**	**0:14:33**
Normal: 0.25	0.870	0.130	0.273	0.597	0.769	0.597	0.612	0:15:45
Normal: 0.20	0.913	0.125	0.273	0.640	0.808	0.656	0.649	0:15:14
Normal: 0.15	0.913	0.125	0.273	0.640	0.808	0.656	0.649	0:15:40
Normal: 0.00	*0.957*	*0.120*	*0.273*	*0.684*	*0.846*	*0.718*	*0.686*	*0:17:01*
Normal: -0.05	0.957	0.214	0.545	0.411	0.759	0.466	0.580	0:17:12
Normal: -0.10	0.957	0.214	0.545	0.411	0.759	0.466	0.580	0:17:24
Normal: -0.15	0.957	0.241	0.636	0.320	0.733	0.373	0.545	0:17:37
Normal: -0.50	*1.000*	*0.258*	*0.727*	*0.273*	*0.742*	*0.337*	*0.548*	*0:20:06*

Cases at -15°C	POD	FAR	PFA	TSS	CSI	HSS	OUI	Avg Lead Time
Normal: 0.25	0.870	0.091	0.182	0.688	0.800	0.672	0.492	0:13:39
Normal: 0.15	0.870	0.091	0.182	0.688	0.800	0.672	0.492	0:14:23
Normal: 0.00	0.913	0.160	0.364	0.549	0.778	0.577	0.531	0:15:50
Normal: -0.05	0.913	0.160	0.364	0.549	0.778	0.577	0.531	0:15:50
Normal: -0.10	*1.000*	*0.148*	*0.364*	*0.636*	*0.852*	*0.703*	*0.687*	*0:15:33*
Normal: -0.20	*1.000*	*0.148*	*0.364*	*0.636*	*0.852*	*0.703*	*0.687*	*0:16:07*
Normal: -0.25	*1.000*	*0.148*	*0.364*	*0.636*	*0.852*	*0.703*	*0.687*	*0:16:32*

Arguably the best statistical results were produced by the normalized -0.10, -0.20, and -0.25 values at -15°C in Table 13. These cases resulted in perfect POD, improved FAR, PFA, TSS, CSI, HSS, OUI, and increased the average lead time compared to the standard. The largest increase in lead time, 1 min. 59 sec, came from normalized -0.25 at -15°C. Additionally, the normalized value of 0.0 at -10°C produced the same POD as the standard, yet improved FAR, PFA, TSS, CSI, HSS, and OUI, while increasing the average lead time by 2 min. 28 sec. Depending on the operational user's requirements, this case might be the most desirable because it produced a 29 sec. increase in average

lead time and improved every skill score except POD when compared to the normalized

-0.25 at -15°C case. If an increase in average lead time is most important, the normalized

-0.5 at -10°C case in Table 13 produced an average lead time of 20 min. 06 sec. This

case was 5 min. 33 sec. better than the standard, produced a perfect POD, maintained

similar skill scores but a higher FA when compared to the standard.

V. Conclusions

5.1 Summary

The goal of this study was to determine the benefits of using DP radar products to forecast CG lightning initiation in an operational setting. This study was accomplished by using DP radar data from KMLB in Melbourne, FL. Lightning initiation forecasting cases, consisting of various DP product combinations, were compared to a conventional radar standard of $Z \geq 40 dBZ$ at -10°C. Over 40 cases that included different values of Z, Z_{DR}, and K_{DP} were tested at both -10°C and -15°C thermal heights. The overall conclusion of this study was that the use of DP products has the potential of improving CG lightning initiation forecasting.

The two cases that produced the most desirable results were $Z \geq 35 dBZ$ combined with $Z_{DR} \geq 0.5 dB$ at -15°C and $Z \geq 30 dBZ$ combined with $Z_{DR} \geq 0.5 dB$ at -10°C. The first case resulted in the best skill score of all cases tested with perfect forecasts of 23 hits, 11 correct negatives, and 0 false alarms or misses. This is the best possible result when forecasting CG lightning. However, an operational user might determine it to be unacceptable because it decreased the average lead time by nearly 5 minutes. The second case is most likely more desirable for an operational user, because it yielded a perfect POD, increased skill score, and increased average lead time by nearly 5 minutes compared to the standard. Normalized cases that combined Z, Z_{DR}, and K_{DP} values also produced desirable results that improved the standard, but were not better than the cases that only combined Z and Z_{DR}.

5.2 Recommendations for Future Work

This study was accomplished to mimic the process an operational forecaster undergoes to forecast CG lightning initiation at the 45 WS; therefore each storm was analyzed individually by the researcher. The amount of information to process in an operational setting is increased when using DP products. This could quickly become a burden of additional work on the forecaster, especially if there are multiple storms in the area that need to be analyzed in a short amount of time, which is often the case near CCAFS/KSC in the summer. Automation could greatly improve a time-constrained forecaster's ability to monitor the area and issue time sensitive WWAs. Furthermore, an automated detection method would eliminate the human error involved in analyzing individual cells. This would also enable the ability to test these cases on a national data set and ultimately include multicellular systems. Although this study shows promising results, testing DP radar algorithms on 34 storms is not enough to create a solid forecasting technique. Testing the best cases from this study on a larger data set has the potential to yield different statistical outcomes, but would be needed in order to verify the results of this initial study.

Future work on this topic should include but is not limited to reanalyzing the data in this study using IC lightning data. CG lightning is not the only concern of the 45 WS, which issues WWAs for IC lightning to allow for additional lead time for personnel safety. A similar study that includes both CG and IC lightning initiation would be beneficial in order to determine if the same cases apply to both. Lastly, the -5°C thermal level should also be considered for study, as well as pairing DP variables from consecutive radar volume scans to determine if additional volume scans produce better

results. The multi-scan approach could guard against storms that do not continue to

develop and possibly reduce false alarms.

References

Barnes, Lindsey R., David M. Schultz, Eve C. Gruntfest, Mary H. Hayden, Charles C. Benight, 2009: CORRIGENDUM: False Alarm Rate or False Alarm Ratio?. Wea. Forecasting, 24, 1452–1454.

Bringi, V. N., K. Knupp, A. Detwiler, L. Liu, I. J. Caylor, and R. A. Black, 1997: Evolution of a Florida thunderstorm during the Convection and Precipitation/Electrification experiment: The case of 9 August 1991. Mon. Wea. Rev., 125, 2131–2160.

Buechler, D. E., and S. J. Goodman, 1990: Echo size and asymmetry: Impact on NEXRAD storm identification. J. Appl. Meteor., 29, 962–969.

Byers, H. R., and R. R. Braham, 1949: The Thunderstorm. Report of the Thunderstorm Project. U.S. Weather Bureau, U.S. Department of Commerce Tech. Rep., 287 pp.

Carey, L. D., and S. A. Rutledge, 1996: A multiparameter radar case study of the microphysical and kinematic evolution of a lightning producing storm. Meteor. Atmos. Phys., 59, 33–64.

Carey, L. D., and S. A. Rutledge, 2000: The relationship between precipitation and lightning in tropical island convection: A C-band polarimetric radar study. Mon. Wea. Rev., 128, 2687–2710.

Church, C.R., 1966: The electrification of hail, Ph.D. thesis, University of Durham.

D'Arcangelo, D. L., 2000: Forecasting the onset of cloud-ground lightning using layered vertically integrated liquid water, M. S. Thesis, Pennsylvania State University, 60 pp.

Deierling, W., Latham, J., W. A. Petersen, S. M. Ellis, and H. J. Christian Jr., 2005: On the relationship of thunderstorm ice hydrometeor characteristics and total lightning measurements. Atmos. Res., 76, 114-126.

Deierling, W., W. A. Petersen, J. Latham, S. Ellis, and H. J. Christian, 2008: The relationship between lightning activity and ice fluxes in thunderstorms, J. Geophys. Res., 113 (D15), D15210, doi:10.1029/2007JD009700.

Doswell III, C.A., 2001: Severe Convective Storms. The American Meteorological Society.

Dye, J. E., J. J. Jones, W. P. Winn, T. A. Cerni, B. Gardiner, D. Lamb, R. L. Pitter, J. Hallett, and C. P. R. Saunders, 1986: Early electrification and precipitation development in a small, isolated Montana cumulonimbus. J. Geophys. Res., 91, 1231-1247.

Dye, J. E., J. J. Jones, A. J. Weinheimer, and W. P. Winn, 1988: Observations within two regions of charge during initial thunderstorm electrification. Quart. J. Roy. Meteor. Soc., 114, 1271–1290.

Dye, J. E., W. P. Winn, J. J. Jones, and D. W. Breed, 1989: The electrification of New Mexico thunderstorms. Part 1: Relationship between precipitation development and the onset of electrification. J. Geophys. Res., 94, 8643–8656.

Goodman, S. J., D. E. Buechler, P. D. Wright, and W. D. Rust, 1988: Lightning and precipitation history of a microburst-producing storm. Geophys. Res. Lett., 15, 1185-1188.

Gremillion M. S., and R. E. Orville, 1999: Thunderstorm characteristics of cloud−to−ground lightning at the Kennedy Space Center, Florida: A study of lightning initiation signatures as indicated by WSR−88D. Wea. Forecasting, 14, 640−649.

GRLevelX, cited 2013: GR2Analyst. [Available online at http://grlevelx.com/gr2analyst/.]

Jameson, A. R., M. J. Rutledge, and E. P. Krider, 1996: Multiple-parameter radar observations of isolated Florida thunderstorms during the onset of electrification. J. Appl. Meteor., 35, 343–354.

Jolliffe, I. T., and D. B. Stephenson, 2003: Forecast Verification: A Practitioner's Guide in Atmospheric Science. John Wiley and Sons.

Keith, W. D., and C. P. R. Saunders. 1990: Further laboratory studies of the charging of graupel during ice crystal interactions. Atmos. Res., 25, 445–464.

Krehbiel, P. R., M. Brook, and R.A. McCrog, 1979: Analysis of the charge structure of lightning discharge to ground. J. Geophys. Res., 84, 2432–2456.

Kumjian, M. R., 2013a: Principles and application of dual-polarization weather radar. Part I: Description of the polarimetric radar variables. J. Operational Meteor., 1 (19), 226-242.

Kumjian, M. R., 2013b: Principles and application of dual-polarization weather radar. Part II: Warm- and cold-season applications. J. Operational Meteor., 1 (20), 243-264.

Kumjian, M. R., 2013c: Principles and application of dual-polarization weather radar. Part III: Artifacts. J. Operational Meteor., 1 (21), 265-274.

Larson, H. R., and E. J. Stansbury, 1974: Association of lightning flashes with precipitation cores extending to height 7 km. J. Atmos. Terr. Phys., 36, 1547–1553.

Lund, N. R., D. R. MacGorman, T. J. Schuur, M. I. Biggerstaff, and W. D. Rust, 2009: Relationships between lightning location and polarimetric radar signatures in a small mesoscale convective system. Mon. Wea. Rev., 137, 4151–4170.

MacGorman, D.R., and W.D. Rust, 1998: The Electrical Nature of Storms. Oxford University Press.

Marshall, T. C., and W. D. Rust, 1991: Electric field soundings through thunderstorms, J. Geophys. Res., 96, 22,297 – 22,306.

Marshall Space Flight Center, cited 2013: Spaceport weather data archive. [Available online at http://trmm.ksc.nasa.gov/.]

Mosier, R. M., C. Schumacher, R. E. Orville, and L. D. Carey, 2011: Radar nowcasting of cloud-to-ground lightning over Houston, Texas. Wea. Forecasting, 26, 199–212.

Murphy, M. J., K. L. Cummins, N. W. S. Demetriades, and W. P. Roeder, 2008: Performance of the new Four Dimensional Lightning Surveillance System (4DLSS) at the Kennedy Space Center/Cape Canaveral Air Force Station Complex. 13th Conference on Aviation, Range, and Aerospace Meteorology, 18 pp.

National Climatic Data Center, cited 2013: HDSS Access System. [Available online at http://has.ncdc.noaa.gov/pls/plhas/has.dsselect.]

Petersen, W. A., S. A. Rutledge, and R. E. Orville, 1996: Cloud-to-ground lightning observations from TOGA COARE: Selected results and lightning location algorithms. Mon. Wea. Rev., 124, 602–620.

Reynolds, S. E., M. Brook, and M. F. Gourley, 1957: Thunderstorm charge separation. J. Met, 14, 426–436.

Roeder, W. P., and C. S. Pinder, 1998: Lightning forecasting empirical techniques for central Florida in support of America's space program. 16th Conference On Weather Analysis And Forecasting, 475-477.

Roeder, W. P., and T. M. McNamara, 2011: Using temperature layered VIL as automated lightning warning guidance. 5th Conference on Meteorological Applications of Lightning Data, Seattle, WA, Paper 688, 10 pp.

Roeder, W. P., T. M. McNamara, B. F. Boyd, J. W. Weems, and S. B. Cocks, 2005: Unique uses of weather radar for space launch. 32nd Conference on Radar Meteorology, 13 pp.

Roeder, W.P. and J.M. Saul, 2012: Four dimensional lightning surveillance system: status and plans. 22nd International Lightning Detection Conference/4th International Lightning Meteorology Conference, Broomfield, CO.

Rogers, R. R., and M. K. Yau, 1989: A Short Course in Cloud Physics. Butterworth-Heinmann Pub.

Rinehart, R. E., 2010: Radar for Meteorologists. 5th ed. Rinehart.

Rutledge, S. A., and W. A. Petersen, 1994: Vertical radar reflectivity structure and cloud-to-ground lightning in the stratiform region of MCSs: Further evidence for in situ charging in the stratiform region. Mon. Wea. Rev., 122, 1760–1776.

Saunders, C. P. R., W. D. Keith, and R. P. Mitzeva, 1991: The effect of liquid water on thunderstorm charging. J. Geophys. Res, 96, 11007–11017.

Takahashi, T., 1978: Riming electrification as a charge generation mechanism in thunderstorms. J. Atmos. Sci, 35, 1536–1548.

Uman, M. A., 1987: The Lightning Discharge. Dover Publications Inc, Mineola, NY.

University of Wyoming, cited 2013: Atmospheric soundings. [Available online at http://weather.uwyo.edu/upperair/sounding.html.]

Vincent, B.R, L.D. Carey, D. Schneider, K. Keeter, and R. Gonski, 2003: Using WSR-88D reflectivity data for the prediction of cloud-to-ground lightning: A North Carolina study. Nat. Wea. Digest, 27, 35-44.

Wallace, J. M., and P. V. Hobbs, 2006: Atmospheric Science: an introductory survey. Academic Press, San Diego, CA, second edition.

Warning Decision Training Branch, cited 2013: Dual-Polarization Radar Training for NWS Partners. [Available online at http://www.wdtb.noaa.gov/courses/dualpol/outreach/.]

Weems, J. W., C. S. Pinder, W. P. Roeder, and B. F. Boyd, 2001: Lightning watch and warning support to spacelift operations. 18th Conference on Weather Analysis and Forecasting, 301-305.

Williams, E. R., 1989: The tripole structure of thunderstorms. J. Geophys. Res., 94, 13151–13167.

Wolf, P., 2006: Anticipating the initiation, cessation, and frequency of cloud-to-ground lightning, utilizing WSR-88D reflectivity data. NWA Electronic Journal of Operational Meteorology, December 2006.

Woodard, C. J., 2011: Operational lightning forecasting technique development and testing utilizing c-band dual-polarimetric radar, Master's thesis, University of Alabaman in Huntsville.

Woodward, C.J., L. D. Carey, W. A. Petersen, and W. P. Roeder, 2012: Operational Utility of Dual-Polarization Variables in Lightning Initiation Forecasting. Electronic J. Operational Meteor, 6, 79-102.

Workman, E. J., and S. E. Reynolds, 1949: Electrical activity as related to thunderstorm cell growth. Bull. Amer. Meteor. Soc.,30, 142–144.

Yang, Y.H., and P. King, 2010: Investigating the potential of using radar echo reflectivity to nowcast cloud-to-ground lightning initiation over southern Ontario. Weather and Forecasting, 25:4, 1235-1248.

Ziegler, C. L., and D. R. MacGorman, 1994: Observed lightning morphology relative to modeled space charge and electric field distributions in a tornadic storm. J. Atmos. Sci., 51, 833–851.

Zipser, E. J., and K. Lutz, 1994: The vertical profile of radar reflectivity of convective cells: A strong indicator of storm intensity and lightning probability? Mon. Wea. Rev., 122, 1751–1759.

Vita

      Captain Kyle R. Thurmond graduated from The Bolles College Preparatory School in Jacksonville, Florida. He entered undergraduate studies at the University of Hawaii at Manoa, Hawaii, where he graduated with a Bachelor of Science degree in Meteorology in May 2009. He was commissioned through the Detachment 175 AFROTC at the University of Hawaii where he was nominated for a Regular Commission. His first assignment was to the 17th Operational Weather Squadron, Hickam AFB, Hawaii, where he served as a weather officer. In May 2012, he entered the Graduate School of Engineering and Management, Air Force Institute of Technology. Upon graduation, he will be assigned to the Ft. Bragg.

REPORT DOCUMENTATION PAGE

1. REPORT DATE *(DD-MM-YYYY)*	2. REPORT TYPE	3. DATES COVERED *(From – To)*
27-03-2014	Master's Thesis	June 2012 – March 2014

4. TITLE AND SUBTITLE		5a. CONTRACT NUMBER
Operational Cloud-to-Ground Lightning Initiation Forecasting Utilizing S-Band Dual-Polarization Radar		
		5b. GRANT NUMBER
		5c. PROGRAM ELEMENT NUMBER
6. AUTHOR(S)		5d. PROJECT NUMBER
Thurmond, Kyle R., Captain, USAF		
		5e. TASK NUMBER
		5f. WORK UNIT NUMBER

7. PERFORMING ORGANIZATION NAMES(S) AND ADDRESS(S)	8. PERFORMING ORGANIZATION REPORT NUMBER
Air Force Institute of Technology Graduate School of Engineering and Management (AFIT/EN) 2950 Hobson Way, Building 640 WPAFB, OH 45433	AFIT-ENP-14-M-36

9. SPONSORING/MONITORING AGENCY NAME(S) AND ADDRESS(ES)	10. SPONSOR/MONITOR'S ACRONYM(S)
45th Weather Squadron 1201 Edward H. White Ste. C-129 Patrick AFB, FL 32925 (321) 853-8410 william.roeder@us.af.mil	45 WS
	11. SPONSOR/MONITOR'S REPORT NUMBER(S)

12. DISTRIBUTION/AVAILABILITY STATEMENT
DISTRIBUTION STATEMENT A. APPROVED FOR PUBLIC RELEASE; DISTRIBUTION IS UNLIMITED

13. SUPPLEMENTARY NOTES
This material is declared a work of the United States Government and is not subject to copyright protection in the United States.

14. ABSTRACT

Previous research on cloud-to-ground (CG) lightning initiation forecasting shows a potential benefit in using dual-polarization (DP) weather radar. The propagation of radio waves in both the horizontal and vertical planes makes DP radar better equipped to identify radar returns indicative of charge separation within clouds. Algorithms using the DP radar products of differential reflectivity (ZDR) and specific differential phase (KDP) combined with reflectivity (Z) values were developed to determine if DP radar could outperform a standard conventional radar forecasting technique ($Z \geq 40dBZ$ at $\neg\neg-10°C$). 68 single-cell thunderstorms were evaluated near Kennedy Space Center (KSC), FL for to develop and test these algorithms. It was concluded that using DP radar to forecast CG lightning provided better results than the standard conventional radar technique through improved skill scores (100% possibility of detection and 0% false alarm ratio), increased lead time (approximately 5 minutes), or both. However, more research over a longer time period is needed to validate these results and convert to an automated operational forecasting tool.

15. SUBJECT TERMS
Cloud-to-Ground, Lightning initiation forecasting, Dual-Polarization Radar

16. SECURITY CLASSIFICATION OF:			17. LIMITATION OF ABSTRACT	18. NUMBER OF PAGES	19a. NAME OF RESPONSIBLE PERSON
					Kevin S. Bartlett, Lt Col, Ph.D, USAF
a. REPORT	**b. ABSTRACT**	**c. THIS PAGE**	UU	72	19b. TELEPHONE NUMBER *(Include area code)*
U	U	U			(937) 255-3636, x 4520 Kevin.bartlett@afit.edu